AD-A182 598 APPROXIMATION TO THE BOUNDARY INTEGRAL EQUATION AND APPLICATIONS TO MODEL.. (U) SIERRA GEOPHYSICS INC KIRKLAND WA J W GIVEN ET AL. FEB 87 AFGL-TR-87-0147 1/1

UNCLASSIFIED F19628-84-C-0104 F/G 20/1 NL

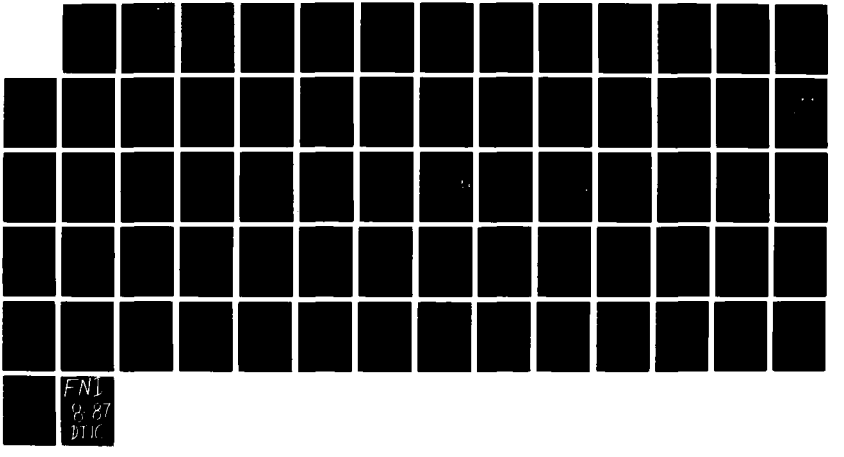

FNI
8-87
DTIC

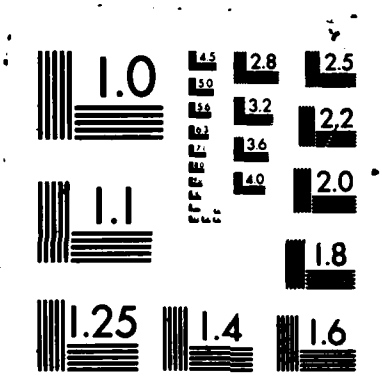

MICROCOPY RESOLUTION TEST CHART
NATIONAL BUREAU OF STANDARDS-1963-A

AFGL-TR-87-0147

SGI-R-87-133

APPROXIMATION TO THE BOUNDARY INTEGRAL EQUATION AND APPLICATIONS TO MODELING ACOUSTIC WAVES IN THREE DIMENSIONAL STRUCTURES

J.W. GIVEN
R.J. APSEL
G.R. MELLMAN
P.C. WONG

SIERRA GEOPHYSICS, INC.
11255 KIRKLAND WAY
KIRKLAND, WASHINGTON 98033

FEBRUARY, 1987

FINAL REPORT
JANUARY 1986 - JANUARY 1987

UNCLASSIFIED
SECURITY CLASSIFICATION OF THIS PAGE

AD-A182 578

REPORT DOCUMENTATION PAGE

1a. REPORT SECURITY CLASSIFICATION: UNCLASSIFIED	1b. RESTRICTIVE MARKINGS
2a. SECURITY CLASSIFICATION AUTHORITY	3. DISTRIBUTION/AVAILABILITY OF REPORT: APPROVED FOR PUBLIC RELEASE; DISTRIBUTION UNLIMITED
2b. DECLASSIFICATION/DOWNGRADING SCHEDULE	
4. PERFORMING ORGANIZATION REPORT NUMBER(S): SIERRA GEOPHYSICS REPORT SGI-R-87-133	5. MONITORING ORGANIZATION REPORT NUMBER(S): AFGL-TR-87-0147
6a. NAME OF PERFORMING ORGANIZATION: SIERRA GEOPHYSICS, INC. (6b. OFFICE SYMBOL (If applicable): 4R088)	7a. NAME OF MONITORING ORGANIZATION: AIR FORCE GEOPHYSICS LAB (AFSC)
6c. ADDRESS (City, State and ZIP Code): 11255 KIRKLAND WAY, SUITE 300 KIRKLAND, WA 98033	7b. ADDRESS (City, State and ZIP Code): HANSCOM AFB, MA 01731
8a. NAME OF FUNDING/SPONSORING ORGANIZATION: ELECTRONIC SYSTEMS DIV/PKR (8b. OFFICE SYMBOL (If applicable): FQ7620)	9. PROCUREMENT INSTRUMENT IDENTIFICATION NUMBER: F19628-84-C-0104
8c. ADDRESS (City, State and ZIP Code): AIR FORCE SYSTEMS COMMAND, USAF HANSCOM AFB, MA 01731	10. SOURCE OF FUNDING NOS: PROGRAM ELEMENT NO. 61102F; PROJECT NO. 2309; TASK NO. G2; WORK UNIT NO. AQ
11. TITLE (Include Security Classification): SEE SECTION 16	

12. PERSONAL AUTHOR(S): J.W. GIVEN, R.J. APSEL, G.R. MELLMAN, P.C. WONG

13a. TYPE OF REPORT	13b. TIME COVERED	14. DATE OF REPORT (Yr., Mo., Day)	15. PAGE COUNT
FINAL	FROM JAN '86 TO JAN '87	1987 FEB	70

16. SUPPLEMENTARY NOTATION: APPROXIMATION TO THE BOUNDARY INTEGRAL EQUATION AND APPLICATIONS TO MODELING ACOUSTIC WAVES IN THREE DIMENSIONAL STRUCTURES

17. COSATI CODES		
FIELD	GROUP	SUB. GR.

18. SUBJECT TERMS (Continue on reverse if necessary and identify by block number): FORWARD MODELING; WAVE PROPAGATION; IRREGULARLY LAYERED MEDIA; BOUNDARY INTEGRAL EQUATION

19. ABSTRACT (Continue on reverse if necessary and identify by block number)

Approximations to the boundary integral equation (BIE) formulation for acoustic wave propagation permits simulation of acoustic waves in layered earth models with three dimensional layer boundaries. The complete BIE solution is approximated by a series expansion analogous to the more familiar generalized ray expansion widely used in seismological modeling. A layer to layer propagation algorithm is presented which is efficient enough to perform three dimensional wave propagation on a modern minicomputer equipped with an array processor. With an efficient propagation algorithm, iterative methods for computing the layer coupling are feasible. The "ray expansion" approach is most useful for approximating solutions on wave propagation problems in which multiple interaction between boundaries can be ignored.

The approximate BIE method is applied to an acoustic model of a mountain in which a flat layered velocity structure is overlain by three dimensional topography. For the solution that includes primary reflection from the layered velocity structure and their corresponding interaction with the topography, amplitude variations between several profiles can be interpreted as they relate to the topography alone.

20. DISTRIBUTION/AVAILABILITY OF ABSTRACT	21. ABSTRACT SECURITY CLASSIFICATION	
UNCLASSIFIED/UNLIMITED ☐ SAME AS RPT ☒ DTIC USERS ☐	UNCLASSIFIED	
22a. NAME OF RESPONSIBLE INDIVIDUAL: JAMES C. BATTIS	22b. TELEPHONE NUMBER (Include Area Code): (617) 377-3767	22c. OFFICE SYMBOL: AFGL/LWH

DD FORM 1473, 83 APR — EDITION OF 1 JAN 73 IS OBSOLETE

UNCLASSIFIED
SECURITY CLASSIFICATION OF THIS PAGE

the profile. The location of the source and receivers on the near surface, low-velocity material introduces strong acoustic waveguide effects equivalent to Love waves in an elastic medium. Modeling these guided waves requires including waves that reflect from the subsurface velocity structure and interact with the free surface several times. These guided waves dominate the solution over the source-receiver geometry of interest. Peak amplitudes vary by a factor of 2 for stations spaced at 1 km; apparently the result of subtle changes in the interference of waves that have interacted with the free surface in different ways. The effect of three dimensional structure on peak amplitudes and waveforms of these guided waves will be difficult to predict.

TABLE OF CONTENTS

LIST OF FIGURES

LIST OF FIGURES

(Continued)

LIST OF FIGURES

(Continued)

LIST OF FIGURES

(Continued)

1.0 SUMMARY

Approximations to the boundary integral equation (BIE) formulation for acoustic wave propagation permit simulation of acoustic waves in layered earth models with three dimensional layer boundaries. The complete BIE solution is approximated by a series expansion analogous to the more familiar generalized ray expansion widely used in seismological modeling. A layer to layer propagation algorithm is presented which is efficient enough to perform three dimensional wave propagation on a modern minicomputer equipped with an array processor. With an efficient propagation algorithm, iterative methods for computing the layer coupling are feasible. The "ray expansion" approach is most useful for approximating solutions on wave propagation problems in which multiple interaction between boundaries can be ignored.

The approximate BIE method is applied to an acoustic model of a mountain in which a flat layered velocity structure is overlain by three dimensional topography. For the solution that includes primary reflection from the layered velocity structure and their corresponding interaction with the topography, amplitude variations between several profiles can be interpreted as they relate to the topography along the profile. The location of the source and receivers on the near surface, low-velocity material introduces strong acoustic waveguide effects equivalent to Love waves in an elastic medium. Modeling these guided waves requires including waves that reflect from the subsurface velocity structure and interact with the free surface several times. These guided waves dominate the solution over the source-receiver geometry of interest. Peak amplitudes vary by a factor of 2 for stations spaced at 1 km; apparently the result of subtle changes in the interference of waves that have interacted with the free surface in different ways. The effect of three dimensional structure on peak amplitudes and waveforms of these guided waves will be difficult to predict.

2.0 INTRODUCTION

Efforts to understand the detailed structure of the earth requires the capability to numerically model seismic wave propagation in complex two- and three-dimensional structures. Computational techniques for modeling wave propagation in complex structures range from simple ray tracing to finite difference and finite element methods. Ray tracing methods are elegant, conceptually simple to grasp, and form the intuitive basis for understanding many types of wave phenomena. As an interpretation and modeling tool, they are indispensible for understanding the results of more complex calculations. For more complete solutions, finite difference methods have received widespread attention (e.g. Alterman and Karal, 1968; Boore, 1972; Kosloff and Baysal, 1982, Vidale, 1986). These methods have large computational requirements and it is not currently feasible to treat three-dimensional problems. Further advances in computer technology, particularly in the development of large parallel machines will remedy this situation. However, alternative approximate methods that provide insight into complex wave phenomena will always be necessary.

One method for posing wave propagation problems, dating from the early nineteenth century, is the Boundary Integral Equation (BIE) technique in which a wavefield in a region of interest is represented by the values of the field and its gradient along a bounding surface. While finite difference methods require sampling the wavefield in all spatial dimensions, the BIE method requires that the wavefield be sampled only along surfaces, which, at first glance, appears to be a huge saving of effort in a three-dimensional problem. However, while the interaction between samples in a finite-difference model is local, the interaction between samples in a BIE representation is global: each point on a surface interacts with every other point on the same surface and the adjacent surfaces. Thus, for complex interaction of several boundaries, (i.e. "lots of multiples" in raytracing terminology) it is not yet clear that the BIE method represents an advantage. However, for problems in which the interaction between boundaries is not severe (i.e. if primaries and low order multiples are of interest), then BIE methods

are an attractive alternative, particularly when propagation over many wavelengths in a homogenous media is involved.

Several treatments of the BIE formulation have appeared in the geophysical literature in recent years. Cole (1980) presented a time-domain formulation for two-dimensional acoustic problems. For many problems of seismological interest, this approach will be unsatisfactory since it is difficult to suppress edge reflections and include realistic attenuation. A frequency-domain treatment of the two-dimensional elastic problem was studied by Ferguson (1982). Both methods failed to handle the interaction integrals efficiently enough to extend the results to three dimensions with current computer technology. Schuster (1984) has studied several approaches to efficiently solving the BIE's. He presents an iterative solution that is directly analogous to familiar ray expansions used in plane-layered media and, thus, has a strong intuitive basis. His formulation lends itself to a variety of useful approximations and hybridizations; it is virtually identical to the approach that we have adopted in the following report.

Apsel et al. (1985, 1983) has formulated a frequency domain approach that is stable, involves no matrix inversions, and that can include the effects of realistic material properties such as attenuation. The formulation is designed to calculate the total response, including all kinematic and dynamic effects using a specially designed pertubation treatment. The method appears to be more cost-effective than finite difference algorithms, however computational demands for a three dimensional model are still much too large for routine treatment.

An attractive feature of the BIE method is that it readily leads to intuitively appealing approximations that allow some hope for understanding complex wavefields in terms of simpler wave propagation concepts such as rays, diffraction, reflection and transmission. An example is the Kirchhoff approximation (Hilterman, 1970; Berryhill, 1979; Scott and Helmberger, 1982; Mellman et al., 1982) in which the BIE equation is broken up into separate calculations for the propagation

between layer interfaces and for the interaction along individual layer boundaries. The self interaction is approximated by treating each point as if the incident wavefield is a plane wave and the interface is a plane oriented along the tangent to the surface at that point. Interaction between two points on the same boundary is not considered and so this approach is only valid if the topography along an interface is not severe enough to introduce multiple scattering; i.e. waves reflected from one part of an interface to another part of the same interface are negligible. For the models that we will treat in this report, we will use this assumption.

In the following, we will first review the BIE formulation as presented in Apsel et al. (1983, 1985) and provide details of some useful approximations. Then we will apply the methods to some realistic calculations to model strong ground motions on a mountain where topography is expected to have significant effects on the wave propagation.

3.0 GENERAL FORMULATION OF BIE METHODOLOGY

The boundary integral equations describing wave propagation through arbitrary three-dimensional elastic multilayered media are derived in two steps. First, wave propagation within a single irregular, homogeneous layer is described by integral representations using the full space Green's functions with properties of that layer. Second, the wavefields in each irregular layer are constrained to interact at the layer boundaries to satisfy all of the boundary and continuity conditions, which leads to a system of integral equations for the unknown boundary values. Once this system of equations is solved for the boundary values, the wavefield may be calculated at all of the receiver positions of interest using the integral representations of the first step.

The model geometry for the wave propagation problem solved in the BIE formulation is depicted in Figure 1 by N irregular layers overlying a semi-infinite half-space. The layers are allowed to pinchout but not to cross in this formulation. Each layer is characterized by constant shear and compressional wave velocities and constant densities. Material attenuation may be introduced by allowing the velocities to be complex. Wave propagation within a given layer is expressed in terms of the Green's functions for a full-space with the properties of that layer. The formulation is not restricted to constant material properties within a given layer, although the Green's functions for that case are quite simple. In the following, the formulation is presented for the acoustic case. Most of the corresponding elastic derivation is presented in Apsel et al. 1983.

In the acoustic case, the field values pressure, P, and particle velocity, $\vec{\delta}$, can be described in terms of a potential, ϕ (see Morse and Feshback, 1953):

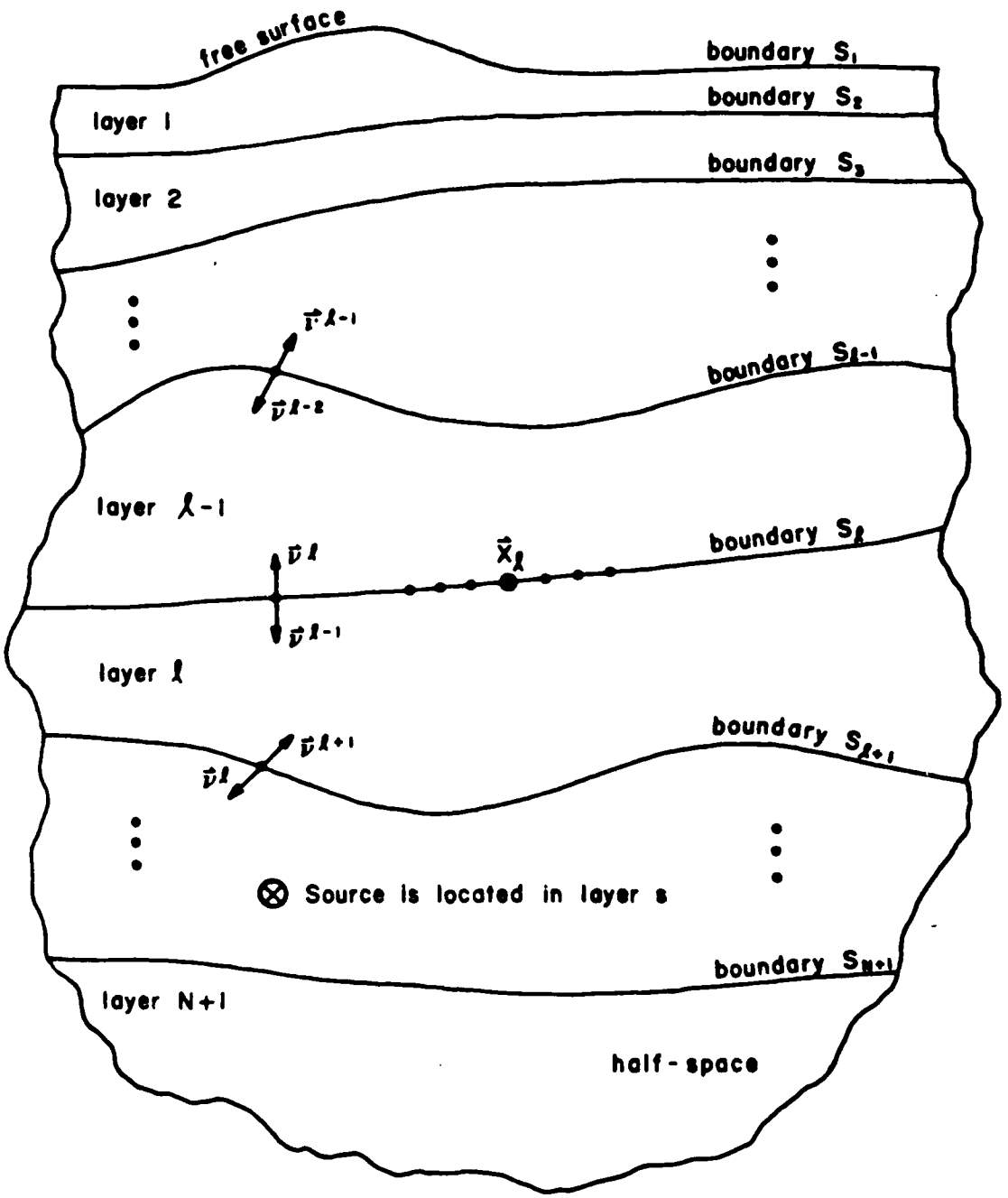

Figure 1. Cross-sectional model geometry for layered half-space used in BIE method formed by N irregular layers overlying a uniform half-space, with each layer characterized by constant material properties. The source and receiver can be located anywhere in the medium.

$$P = \frac{\partial}{\partial t} \phi$$

$$\vec{\delta} = \frac{1}{\rho} \nabla \phi$$

The potential, ϕ, then satisfies the wave equation:

$$\nabla^2 \phi - \frac{1}{\alpha^2} \frac{\partial^2 \phi}{\partial t^2} = 0 \qquad (1)$$

where α is the acoustic velocity and ρ is the density.

If we define the Fourier transform with respect to time as

$$\phi(\vec{x},\omega) = \int_{-\infty}^{\infty} \phi(\vec{x},t)\, e^{+i\omega t}\, dt$$

then we have the Helmholtz equation

$$\nabla^2 \phi + k^2 \phi = 0 \qquad (2)$$

with $k^2 = \omega^2/\alpha^2$.

The first step in the formulation is to write expressions for the potential field within a single layer without consideration of the boundary interaction. In layer ℓ (ℓ=1,2,...,N+1), the potential must satisfy the homogeneous ($\ell \neq s$) or inhomogeneous (ℓ=s) equations of motion (depending on whether or not the source is located in layer ℓ) for a full-space with properties of layer ℓ. The Kirchhoff integral

representation (e.g. Stratton, 1948) or, equivalently, the Representation Theorem of Elastodynamics (deHoop, 1958) provide an expression for the potential located anywhere within volume V_ℓ containing layer ℓ in terms of integrals of the potential and its normal field over the bounding surface of volume V_ℓ multiplied by the corresponding Green's functions for a full-space with properties of that layer. The potential at location $\vec{x}_\ell$ can then be written in the frequency domain using the integral representation for a volume V_ℓ bounded by layer interfaces S_ℓ and $S_{\ell+1}$.

$$\varepsilon^\ell(\vec{x}_\ell)\phi(\vec{x}_\ell) = \iint_{S_\ell} \Big[G^\ell(\vec{x}_\ell,\vec{y}_\ell)\,\psi^\ell(\vec{y}_\ell) - H^\ell(\vec{x}_\ell,\vec{y}_\ell)\,\phi^\ell(\vec{y}_\ell) \Big] dS(\vec{y}_\ell)$$

$$- \iint_{S_{\ell+1}} \Big[G^\ell(\vec{x}_\ell,\vec{y}_{\ell+1})\psi^{\ell+1}(\vec{y}_{\ell+1}) - H^\ell(\vec{x}_\ell,\vec{y}_{\ell+1})\phi^{\ell+1}(\vec{y}_{\ell+1}) \Big] dS(\vec{y}_{\ell+1})$$

$$+ \delta_{\ell s} \iiint_{V_\ell} \Big[G^\ell(\vec{x}_\ell,\vec{z}_\ell) f(\vec{z}_\ell) \Big] dV(\vec{z}_\ell) \qquad (3)$$

in which the frequency arguments have been omitted for brevity and

$\vec{y}_m$ = an integration point on bounding surface S_m;

$G^{\ell}(\vec{x}_{\ell}, \vec{y}_m)$ = the full-space Green's function for the potential ϕ at location y_m on surface S_m due to point force in the i-direction at location $\vec{x}_{\ell}$ with properties of layer ℓ;

$\psi^{\ell}(\vec{y}_m)$ = $\nabla\phi^{\ell}(\vec{y}_m) \cdot \vec{v}(\vec{y}_m)$

$H^{\ell}(\vec{x}_{\ell}, \vec{y}_m)$ = $\nabla_y G^{\ell}(\vec{x}_{\ell}, \vec{y}_{\ell}) \cdot \vec{v}(\vec{y}_{\ell})$

$f(\vec{z}_{\ell})$ = the source function at location z_{ℓ} anywhere in layer ℓ (assuming the source is a Delta-function in space, then the volume integral reduces to the evaluation of the integrand at point $\vec{z}_{\ell}$);

$\delta_{\ell s}$ = 0, if ℓ=s
1, if ℓ=s ,s = source layer number;

$\varepsilon^{\ell}(\vec{x}_{\ell})$ =
1, if $\vec{x}_{\ell}$ inside layer ℓ
½, if $\vec{x}_{\ell}$ on surface bounding layer ℓ
0, if $\vec{x}_{\ell}$ outside layer ℓ

In Eq. (1), the layer comprising volume V_{ℓ} is assumed to extend to infinity at the horizontal extremes to eliminate the surface integrals along those portions of the surface bounding volume V_{ℓ} and the negative sign for the integral over surface $S_{\ell+1}$ is associated with using the upward normal $\vec{v}^{\ell+1} = -\vec{v}^{\ell}$ in the definition of the traction components. Once the boundary values for $\phi(\vec{y}_m)$ and $\psi(\vec{y}_m)$ are determined for bounding interfaces S_{ℓ} and $S_{\ell+1}$, Eq. (1) can then be used to obtain the displacement field at any point $\vec{x}_{\ell}$ within layer ℓ. Expressions for the full-space elastic Green's functions with constant

material properties are given in Appendix A of Apsel et al., 1983 for two and three dimensional wave propagation in elastic as well as acoustic media. This completes the propagation step of the BIE formulation and it remains to impose the boundary interaction coupling.

The boundary interaction coupling requires simultaneous satisfaction of a pressure-free surface (interface 1) and both continuous pressure and normal components of velocity across each layer interface (2,3,...,N+1). The coupled boundary integral equations arising from the continuity conditions across each layer interface, S_ℓ (ℓ=2,3,...,N+1), are obtained by evaluating Eq. (4) in volumes $V_{\ell-1}$ and V_ℓ (layers ℓ-1 and ℓ) at a discrete number (q_ℓ) of observations $\vec{x}_\ell$ along common surface S_ℓ and imposing the boundary conditions:

$$\phi^{\ell-1}(\vec{x}_\ell) = \phi^{\ell}(\vec{x}_\ell) \quad \text{and} \quad \frac{1}{\rho_{\ell-1}} \psi^{\ell-1} = \frac{1}{\rho_\ell} \psi^{\ell}$$

for all quadrature points $\vec{y}_\ell$ on surface S_ℓ. To derive an integral representation for ϕ when ϕ is on the boundary requires special treatment of the singularities present in the Green's functions G^ℓ and H^ℓ. Integration of the singularities is straightforward and is discussed in work by Scott (1985), Cole (1980) and Banaugh (1962).

The resulting set of equations, for ℓ = 1 to N+1, are

$$\tfrac{1}{2}\phi^{\ell}(\vec{x}_{\ell}) = \int_{S_{\ell-1}}\Big[G^{\ell-1}(\vec{x}_{\ell},\vec{y}_{\ell-1})\,\psi^{\ell-1}(\vec{y}_{\ell-1}) - H^{\ell-1}(\vec{x}_{\ell},\vec{y}_{\ell-1})\;\phi^{\ell-1}(\vec{y}_{\ell-1})\Big]\,dS(\vec{y}_{\ell-1})$$

$$-\int_{S_{\ell}}\Big[G^{\ell-1}(\vec{x}_{\ell},\vec{y}_{\ell})\psi^{\ell-1}(\vec{y}_{\ell}) - H^{\ell-1}(\vec{x}_{\ell},\vec{y}_{\ell})\,\phi^{\ell-1}(\vec{y}_{\ell})\Big]\,dS(\vec{y}_{\ell}) + \delta_{\ell-1s}F(\vec{x}_{\ell}) \qquad (4)$$

and

$$\tfrac{1}{2}\phi^{\ell}(\vec{x}_{\ell}) = \int_{S_{\ell}}\Big[G^{\ell}(\vec{x}_{\ell},\vec{y}_{\ell})\psi^{\ell}(\vec{y}_{\ell}) - H^{\ell}(\vec{x}_{\ell},\vec{y}_{\ell})\phi^{\ell}(\vec{y}_{\ell})\Big]\,dS(\vec{y}_{\ell})$$

$$-\int_{S_{\ell+1}}\Big[G^{\ell}(\vec{x}_{\ell},\vec{y}_{\ell+1})\psi^{\ell}(\vec{y}_{\ell+1}) - H^{\ell}_{ji}(\vec{x}_{\ell},\vec{y}_{\ell+1})\,\phi^{\ell}(\vec{y}_{\ell+1})\Big]\,dS(\vec{y}_{\ell+1}) \qquad (5)$$

$$+\,\delta_{\ell s}F(\vec{x}_{\ell}) \qquad (i,j=1,2,3),\ (\ell=2,3,\ldots,N+1).$$

where $F(\vec{x}_{\ell}) = \int_{V_{\ell}} G^{\ell}(\vec{x}_{\ell},\vec{z}_{\ell})f(\vec{z}_{\ell})\,dV(\vec{z}_{\ell})$.

Equations (4) and (5) represent a simultaneous set of $2q_\ell$ Fredholm integral equations of the second kind for the same number of unknown boundary values, ϕ^ℓ and ψ^ℓ on surface S_ℓ, which are coupled to the unknown boundary values on surface $S_{\ell-1}$ and $S_{\ell+1}$ through the integrals over surfaces $S_{\ell-1}$ and $S_{\ell+1}$, respectively. Note that when ℓ=1 or ℓ=2 in Eq. (4), then the term involving $\phi^1(\vec{y}_1)$ is identically zero because of the tractionless free-surface conditions. Also, note that when ℓ=N+1 in Eq. (5), then the integral over surface $S_{\ell+1}$ vanishes by virtue of the radiation conditions implicit in the Green's functions for the underlying semi-infinite space. Boundary integral equations (4) and (5) are evaluated at a discrete set of q_ℓ example points $\vec{x}_\ell$ on each boundary S_ℓ with sample points from one boundary becoming Green's function quadrature points for the next boundary. When completely discretized, Equations (4) and (5) represent a coupled system of singular Fredholm integral equations of the second kind for the unknown boundary values along all layer boundaries. Singularities occur in the Green's functions when quadrature point $\vec{y}_m$ approaches observation point $\vec{x}_m$ in the second integral in Eq. (4) and the first integral in Eq. (5). Singularities can also occur in the Green's functions when two adjacent layer boundaries intersect and would be evidenced in the first integral in Eq. (4) or the second integral of Eq. (5), depending on where the intersections occur.

To compute a numerical approximation to (5) we discretize the integral equations to form matrix operations. First it is convenient to introduce some additional shorthand:

$$G^m_{ij}\,\psi_j = G^m(\vec{x}_i, \vec{y}_j)\,\psi(\vec{y}_j)\,dS(\vec{y}_j)$$

$$H^m_{ij}\,\phi_j = H^m(\vec{x}_i, \vec{y}_j)\,\phi(\vec{y}_j)\,dS(\vec{y}_j)$$

where G^m_{ij}, H^m_{ij} are the Green's functions giving the response at point $\vec{x}$ on the i'th layer due to a source at point $\vec{y}$ on the jth layer with

acoustic properties α_m, ρ_m, (m = i or j). The forcing term can be written as

$$F_{ij} = \int_V f(z_j)\, G^j(\vec{x}_i, \vec{z}_j)\, dZ_j$$

where F_{ij} is the response at point x on boundary i due to a distribution of sources on $\vec{z}$ in the j^{th} layer.

We define submatrices, D (downgoing) and U (upgoing):

$$D_{\ell\ell-1} = \begin{bmatrix} -H^{\ell-1}_{\ell\ell-1} & G^{\ell-1}_{\ell\ell-1} \\ 0 & 0 \end{bmatrix}$$

$$U_{\ell\ell+1} = \begin{bmatrix} 0 & 0 \\ H^{\ell}_{\ell\ell+1} & -G^{\ell}_{\ell\ell+1} \end{bmatrix}$$

the boundary interaction matrix:

$$B_{\ell\ell} = \begin{bmatrix} H^{\ell-1}_{\ell\ell} & -G^{\ell-1}_{\ell\ell} - 1/2\, I \\ -H^{\ell}_{\ell\ell} & G^{\ell}_{\ell\ell} - 1/2\, I \end{bmatrix}$$

and the forcing function matrix:

$$F_\ell = \begin{bmatrix} F_{\ell-1\ \ell} \\ F_{\ell\ \ell} \end{bmatrix}$$

where I is the identity matrix.

The unknown boundary values are written:

$$\Phi_\ell = \begin{bmatrix} \phi_\ell \\ \psi_\ell \end{bmatrix}$$

Then the integral equation (5) can be written as a system of equations:

$$\begin{bmatrix} F_1 \\ \cdot \\ \cdot \\ \cdot \\ F_{N+1} \end{bmatrix} = \begin{bmatrix} B_{11} & U_{12} & & \\ D_{21} & B_{22} & U_{23} & \\ & \cdot & & \\ & & \cdot & \\ & & & D_{N+1N}\ B_{N+1\ N+1} \end{bmatrix} \begin{bmatrix} \Phi_1 \\ \Phi_2 \\ \cdot \\ \cdot \\ \cdot \\ \Phi_{N+1} \end{bmatrix} \quad (6)$$

Note that the free surface boundary conditions can be included by explicitly constraining Φ_1

$$\Phi_1 = \begin{pmatrix} 0 \\ \Psi_1 \end{pmatrix}$$

and that the radiation conditions are explicitly included by not allowing any upgoing waves from the N+1 region.

Despite a simple form, Equation (6) represents a formidable computational effort. Each submatrix is dense and for problems of seismological interest, say with grids of 1000 x 1000 nodes, when propagation over many wavelengths is of interest, the U, D, and B matrices are of order $10^6 \times 10^6$ in size. Obviously this formulation is only of symbolic utility and some approximations are necessary. Furthermore, decomposition into simpler, although approximate, methods is useful from the standpoint of understanding the complex wave interactions in terms of the physical parameters of the model.

Several ways to approximate a solution to Equation (6) may be suggested by considering simple iterative solutions to ordinary systems of equations of the same form. Formally, these solutions are known as Born approximations (Schuster, 1983) but here we use a heuristic approach to develop the same ideas.

Consider the well known Gauss-Seidel iteration method for ordinary linear equations where the i^{th} iteration is given by:

$$\Phi_{\ell}^{(i)} = B_{\ell\ell}^{-1} \left[F_{\ell} - D_{\ell\ell-1} \Phi_{\ell-1}^{(i-1)} - U_{\ell\ell+1} \Phi_{\ell+1}^{(i-1)} \right] \qquad (7)$$

Now, on the first iteration, Φ_{ℓ}^{0} is set equal to 0. Beginning on the first row and moving downward, Φ_{ℓ} remains 0 for $\ell<s$ where s contains a source. At that layer

$$\Phi_{s}^{(1)} = B_{ss}^{-1} \left(F_{s} \right)$$

and $$\Phi_{s+1}^{(1)} = B_{s+1s+1}^{-1} \left(F_{s+1} - D_{s+1s} \Phi_{s}^{(1)} \right)$$

and so on through the layers:

$$\Phi_{N+1}^{(1)} = B_{N+1\ N+1}^{-1} D_{N+1\ N} \Phi_{N}^{(1)}$$

At the end of the first iteration down through the layers, we calculate the second iteration from the N+1 interface up through the layers

$$\Phi_{\ell}^{(2)} = B_{\ell\ell}^{-1} U_{\ell\ell+1} \Phi_{\ell+1}^{(2)} .$$

This formulation can be recognized as very similar to a ray expansion with the U and D operators propagating the wavefield from one interface to the next and the $B_{\ell\ell}^{-1}$ determining the transmitted and reflected wave field at each interface. It is identical to the Generalized Born Series approach described by Schuster (1984). If the layer interfaces are horizontal, the wavefield can be Fourier transformed into a horizontal wavenumber spectra and the convolution operators U, D, and B^{-1} can be easily computed and applied for each wavenumber. The matrix equation then reduces to the familiar propagator formulation as described in textbooks on seismology (e.g. Aki and Richards, 1980). In general, however, application of each of these operators represents a convolution in either the spatial or wavenumber domains. Each convolution requires on the order of q^2 operations where q is the number grid nodes on each surface. For a model of grid size 10^3 x 10^3, this represents 10^{12} operations. Clearly further approximations to each of the operators are necessary.

4.0 APPROXIMATIONS TO $D_{\ell-1\ell}$, $U_{\ell\ell+1}$

To propagate a wavefield Φ_ℓ from one layer boundary to an adjacent layer boundary, we will use a Fourier transform method. Consider the situation in Figure 2 in which we wish to propagate Φ_ℓ to layer boundary $\ell+1$. If the layer boundaries ℓ and $\ell+1$ were horizontal we could apply a two dimensional Fourier transform and propagate the wavefield by simple multiplication in the wavenumber domains.

The use of FFT's to compute the wave number spectra of the wavefield allows us to calculate this operation in order n log n operations, where n is the number of points defining the boundary, a large savings over the explicit n^2 operations in the (x, y, z) domain.

Now consider the surface z_ℓ (x,y), a single-valued function of x and y and $\Phi_\ell(x,y)$, the sampled wavefield. We sample $\Phi_\ell(x,y)$ along the intersection of $z_\ell(x,y)$ and a horizontal plane ξ_k = constant:

$$\Phi'_\ell(x,y,\xi_k) = \Phi_\ell(x,y,z_\ell) \left(\frac{\Delta\xi - |z_\ell - \xi_R|}{\Delta\xi} \right) \frac{1}{v_z} \quad dx\,dy$$

$$\text{for } \xi_k - \Delta\xi \leq z_\ell \leq \xi_k + \Delta\xi \qquad (8)$$

$$= 0 \text{ for } z_\ell \text{ otherwise.}$$

where $\Delta\xi$ is the distance between planes on which a sampling of Φ_ℓ is desired and v_z is the z component of the surface normal. If Φ_ℓ (x,y,z_ℓ) is sampled over K horizontal planes such that $\xi_1 < z_\ell < \xi_K$ then

$$D_{\ell+\ell}\,\Phi_\ell\,(x,y,z_\ell) = \int \left(-H^\ell_{\ell+1\ell}\,\Phi_\ell + G^\ell_{\ell+1\ell}\,\nabla\Phi_\ell \cdot \vec{v} \right) dS =$$

$$\sum_{k=1}^{K} D_{\ell+1\ k}\,\Phi'(x,y,\xi_k) \qquad (9)$$

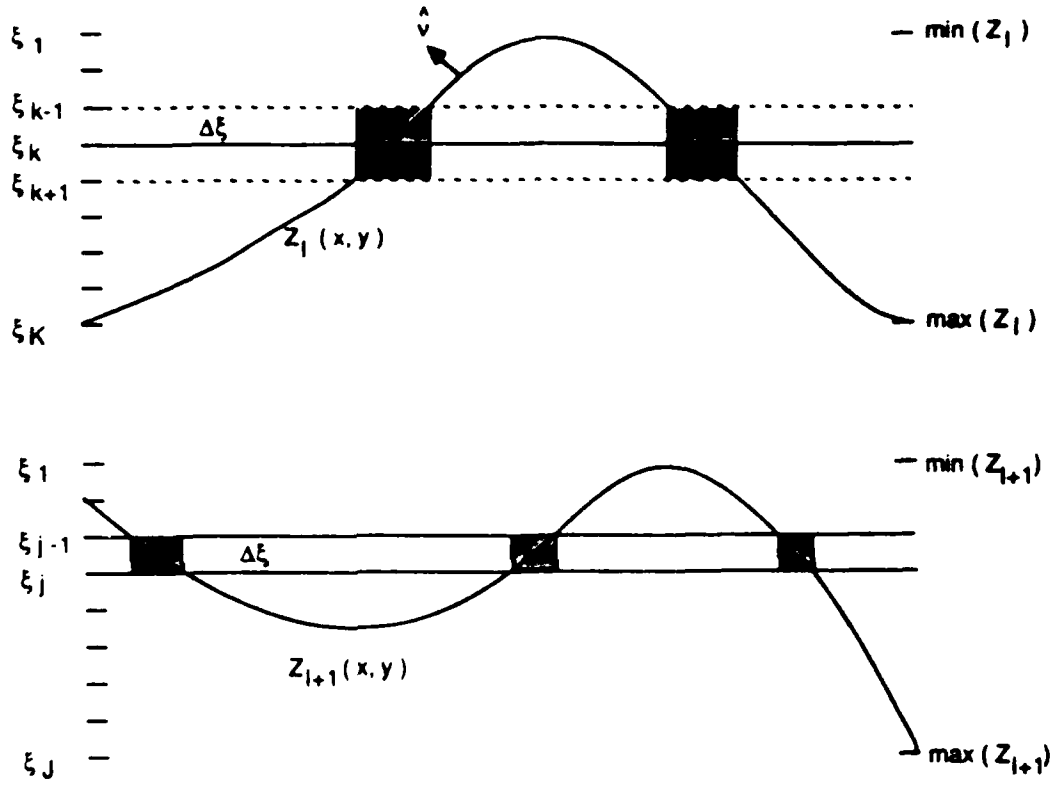

Figure 2. Cross-section description of propagation algorithm. Field values ϕ and $\nabla\phi\cdot\vec{v}$ for $\xi_{k-1} < z_\ell < \xi_{k+1}$ (shaded regions) are projected onto a plane ξ_k = constant. The project field values are the propagated, using Fourier transform techniques to each plane ξ_j (j=1,J) on surface $z_{\ell+1}(x,y)$ and projected onto $z_{\ell+1}$.

where now $D_{k\ell}$ represents the operator that propagates Φ from horizontal level ξ_k to layer ℓ.

After representing $\Phi_\ell\ (x,y,z_\ell)$ in terms of field values on horizontal planes, we propagate these field values to horizontal planes ξ_j, $\xi_j - \Delta\xi \leq z_{\ell+1} \leq \xi_j + \Delta\xi$ and use these field values to estimate the actual values of $\Phi_{\ell+1}$ on $z_{\ell+1}$ using a simple linear interpolation method that is the inverse of (8) above.

Clearly, the number of operations needed to propagate the wavefield to or from a surface is directly related to the relief on the layer. Since the sampling and interpolating is analogous to that used in some simple finite difference schemes, a sample interval of about 10 levels per wavelength will be necessary. Therefore if the total relief is comparable to many wavelengths, this technique becomes less advantageous. However, it should be remembered that in our frequency domain formulation, the sampling can be adapted to the frequency of interest, with only coarse sampling necessary for the low frequencies. Nevertheless for most problems of seismological interest, variation in the vertical direction is much less than the horizontal dimensions; handling wave propagation in homogeneous layers using this technique may allow us to treat a limited set of realistic models without requiring a super-computer.

5.0 APPROXIMATION TO $B_{\ell\ell}^{-1}$

The operator $B_{\ell\ell}$ is very large and completely dense (no non-zero elements). Calculating the inverse directly is not feasible in three dimensions; even calculating the elements and applying the operator directly is barely manageable. We will apply the propagation scheme described in the last section to compute $B_{\ell\ell}\ \Phi_\ell$, which may provide an iterative means of calculating $B_{\ell\ell}^{-1}\ \Phi_\ell$.

Consider a field incident on a boundary ℓ, from the ℓ-1 layer, with field values ϕ^o, $\nabla\phi^o\cdot\vec{v}$. Further suppose that we have an estimate of the boundary values $\phi^\ell(\vec{x}) = \phi^e(\vec{x})$ and $\nabla\phi^e(\vec{x})\cdot\vec{v}$. An initial estimate may be $\phi^e(\vec{x}) = \phi^o(\vec{x})$. Then the discretized boundary interaction equations can be written

$$\begin{aligned} 1/2\ \phi_i^\ell &= -G_{ij}^{\ell-1}\ (a\ \nabla\phi^{e\vec{}}\cdot\vec{v})_j + H_{ij}^{\ell-1}(b\ \phi^e)_j + \phi_i^o \\ 1/2\ \phi_i^\ell &= G_{ij}^{\ell}\ (a\ \nabla\phi^{e\vec{}}\cdot\vec{v})_j - H_{ij}^{\ell}\ (b\ \phi^e)_j \end{aligned} \qquad (10)$$

where $(b\phi^e)_j = b(\vec{y}_j)\ \phi^e(y_j)$, and the function $a(\vec{y})$ is defined similarly. A similar set of equations is implied for $\nabla\phi_i^\ell\cdot\vec{v}$:

$$\begin{aligned} 1/2\ \nabla\phi_i^\ell\cdot\vec{v} &= \vec{v}\cdot\nabla\left(-G^{\ell-1}_{ij}\ (a\nabla\phi^e\cdot\vec{v})_j + H_{ij}^{\ell-1}\ (b\phi^e)_j\right) + \nabla\phi_i^o\cdot\vec{v}_i \\ 1/2\ \nabla\phi_i^\ell\cdot\vec{v} &= \vec{v}_i\cdot\nabla\left(G_{ij}^{\ell}\ (a\nabla\phi^e\cdot\vec{v})_j - H_{ij}^{\ell}\ (b\phi^e)_j\right) \end{aligned} \qquad (11)$$

We propose to iteratively solve Equation (10) by assuming (1) that the ϕ_i^{ℓ} depends largely on $a(\vec{y})$ and $b(\vec{y})$ near $\vec{y} = \vec{x}_i$, and (2) that $a(\vec{y})$ and $b(\vec{y})$ are slowly varying functions. Then we can write

$$\begin{aligned} 1/2\ \phi_i^{\ell} &= -a_{(i)}\ g_i^{\ell-1} + b_{(i)}\ h_i^{\ell-1} + \phi^o \\ 1/2\ \phi_i^{\ell} &= a_{(i)}\ g_i^{\ell} - b_{(i)}\ h_i^{\ell} \end{aligned} \qquad (12)$$

where (i) indicates no summation is implied over i.

In Equation 12, g_i^n, h_i^n are defined by

$$g_i^n = G_{ij}^n\ (\nabla\phi^e \cdot \vec{v})_j$$

$$h_i^n = H_{ij}^n\ \phi_j^e$$

For Equation 11 we have

$$1/2\ \nabla\phi_i^{\ell} \cdot \vec{v}_i = -a_i\ \vec{v}_i \cdot \nabla\ g_i^{\ell-1} + b_i \vec{v}_i \nabla\ h_i^{\ell-1} + \nabla\phi \cdot \vec{v}$$

$$1/2\ \nabla\phi_i^{\ell} \cdot \vec{v}_i = a_i\ \vec{v}_i \cdot \nabla g_i^{\ell} - b_i\ \vec{v}_i \cdot \nabla\ h_i^{\ell}$$

The key assumption in the above manipulations is the removal of the unknown functions $a(\vec{y})$ and $b(\vec{y})$ from the convolution of the Green's functions, G_{ij} and H_{ij}, with the estimated field values ϕ^e and $\nabla\phi^e \cdot \vec{v}$. These convolutions can now be computed in a way exactly analogous to the methods described in the previous section.

Now the continuity conditions at the boundary give two equations for the unknowns a_i and b_i at each grid point, which will define the functions $a(\vec{x})$ and $b(\vec{x})$ necessary to update estimates of the field values.

By applying the boundary conditions to ϕ_i and $\nabla\phi_i^{\ell}\cdot\vec{v}_i$, we can solve for the function $a(\vec{x})$, $b(\vec{x})$ for all surface points providing a new estimate

$$\phi^{e}_{new}(\vec{x}) = a(\vec{x})\,\phi^{e}_{old}(\vec{x}) \text{ and } \nabla\phi^{e}_{new}(\vec{x})\cdot\vec{v} = \nabla\phi^{e}_{old}(\vec{x})\cdot\vec{v}$$

The procedure is then iterated several times. The propagation methods discussed in the previous section to propagate field values from layer to layer can be extended to propagate field values between different areas of the same interface. The above iterative solution has undergone only preliminary exploration and thus its convergence properties are currently unknown. It is an appropriate way to start investigating methods to solve the boundary interaction problem given a computationally feasible way to apply the operator $B_{\ell\ell}$.

The models provided by AFGL that we will use in the subsequent sections of this report require no elaborate approximations to $B^{-1}_{\ell\ell}$. The only layer boundary that varies in these dimensions is the free surface boundary. Furthermore, the topography is smooth enough to permit some reasonable approximations that represent huge saving in the calculations. At the free surface, the boundary condition is ϕ=o. We make the further assumption that $\nabla\phi^{R}\cdot\vec{v} = -\nabla\phi^{o}\cdot\vec{v}$, where the superscript, R, designates the reflected field and o, the incident field. This assumption neglects energy that may reflect several times off of the surface during a single interaction, such as in the "whispering gallery" effect. This approximation is identical to the Kirchhoff-Helmholtz approximation as described by Scott and Helmberger (1983).

6.0 AFGL MODEL CALCULATIONS

The earth structures used for the wave propagation studies are from Cipar (Personal Comm.) and referred to as Generic Mountain, model 1 and model 2. Table 1 gives the model parameters, the S-wave velocity being irrelevant for our purposes because we are dealing with acoustic waves (i.e., we assume that the model is a fluid). The three dimensional variation of the model is confined to the free surface; the lower layers are flat. As discussed earlier, this feature greatly simplifies the calculations since propagation and interaction between flat layers can be handled with Fourier transforms.

Figure 3 gives a contour map of the surface, and Figures 4, 5, and 6 show several cross-sections through the model. The actual model used in the calculation is a smoothed version of that provided by Cipar (Personal Comm.). The contours were digitized, and converted to a regularly sampled grid using a surface inversion algorithm that determines the smoothest unaliased surface that fits the data values. This gridding method removes the sharp corners found in the model as described by Cipar (Personal Comm.) and creates a model more suitable for numerical calculations.

The source locations and receiver arrays are shown in Figure 4 and described in Table 2. In addition to the receiver arrays specified by AFGL we have computed several profiles at the receiver depth in the directions of the receivers arrays. These profiles are useful for identifying the origin of the arrivals based upon the moveout of the various phases.

The maximum feasible grid size for the calculation is currently 128 x 128. To obtain the maximum frequency bandwidth we performed the calculations using two different grid node spacing depending upon the frequency. A single grid with node spacing of 0.24 km was used to calculate the response at the three profiles from 0 to 5.4 hz. For higher frequencies, 5.6 to 11 hz, separate grids were used; one for the

TABLE 1

MODEL 1

LAYER	SEISMIC VELOCITY P-WAVE	SEISMIC VELOCITY S-WAVE	DENSITY g/cm^3	
1	2.6	1.49	2.65	mountain
2	3.2	1.86	2.65	basement
3	6.0	3.50	2.80	granite

MODEL 2

1	2.60	1.49	2.65	caprock
2	2.21	1.27	2.25	low velocity
3	3.20	1.86	2.65	basement
4	6.00	3.50	2.80	granite

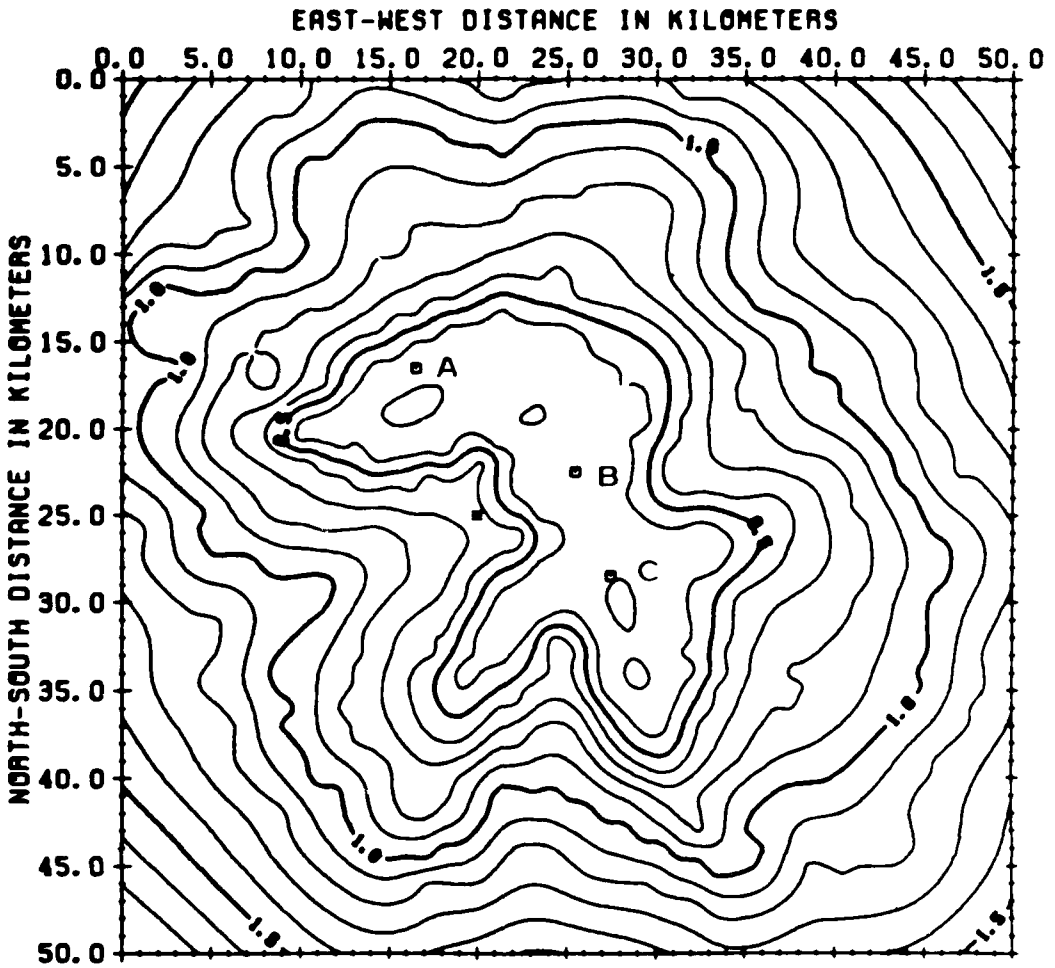

FIGURE 3. Contour map of surface topography of generic mountain model. Depth units are in km.

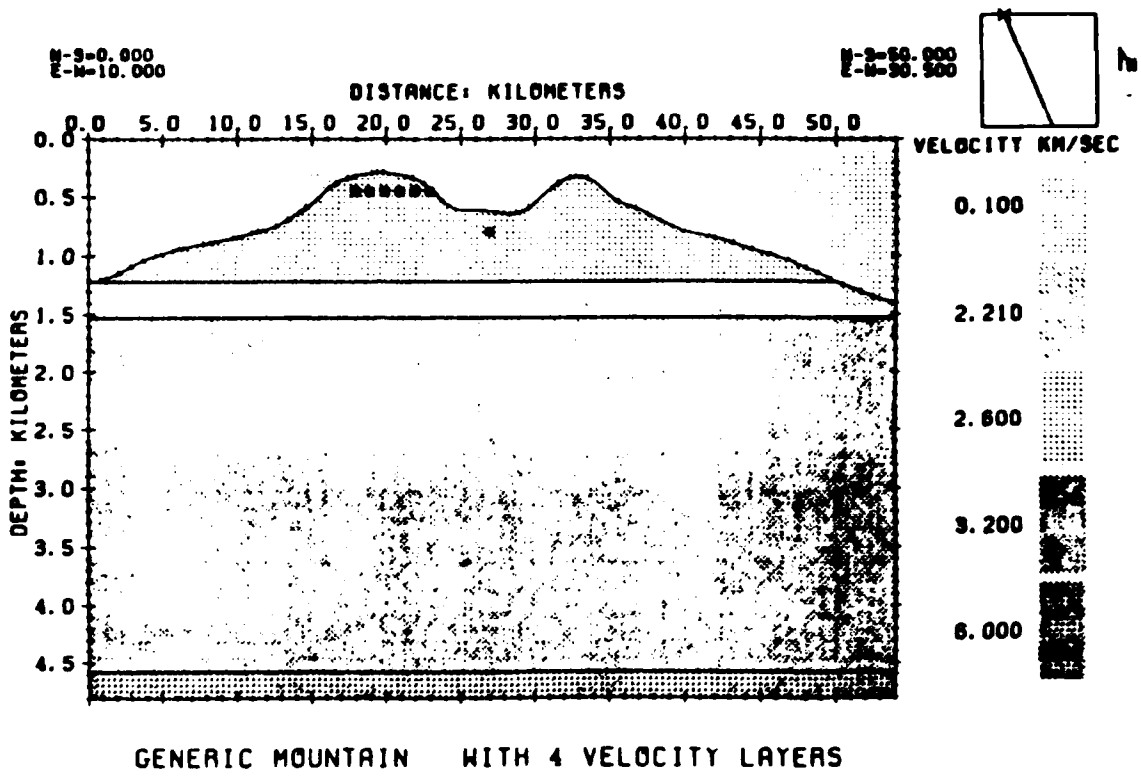

GENERIC MOUNTAIN WITH 4 VELOCITY LAYERS

FIGURE 4. Cross section of model 2 along profile A. Model 1 is identical except that the material properties in layer 3 are the same as layer 2; i.e., there is no low velocity zone.

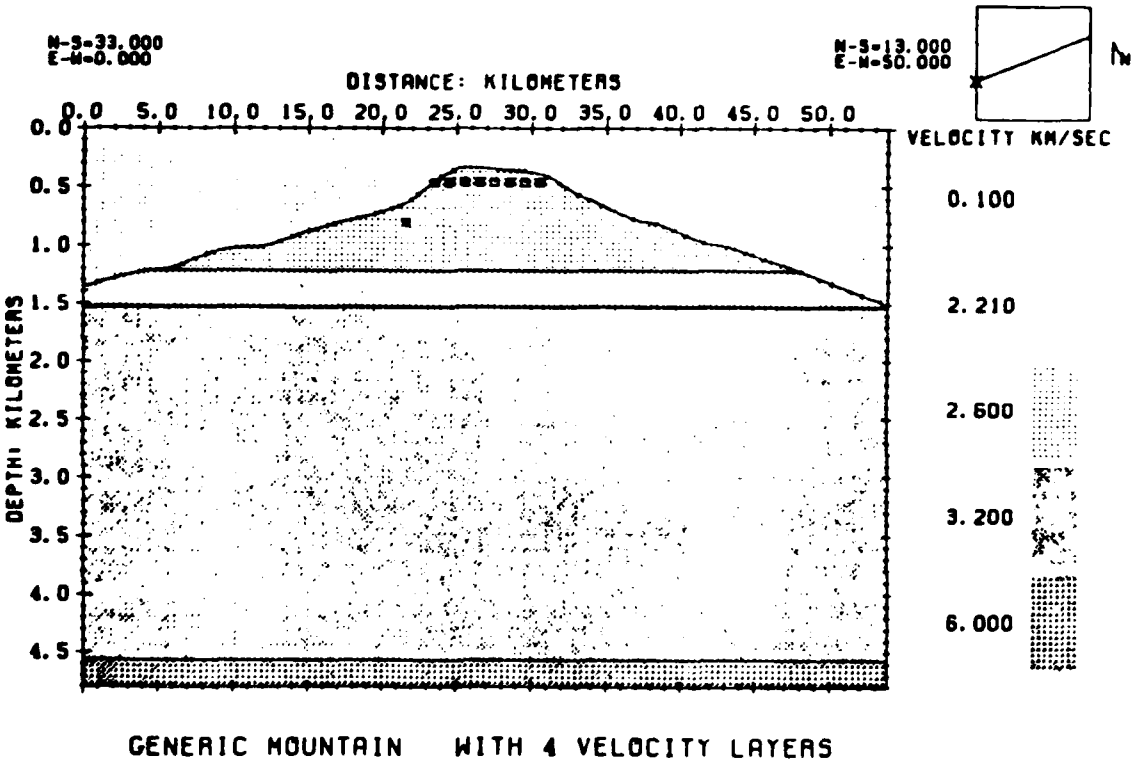

FIGURE 5 Cross section of model 2 along profile B.

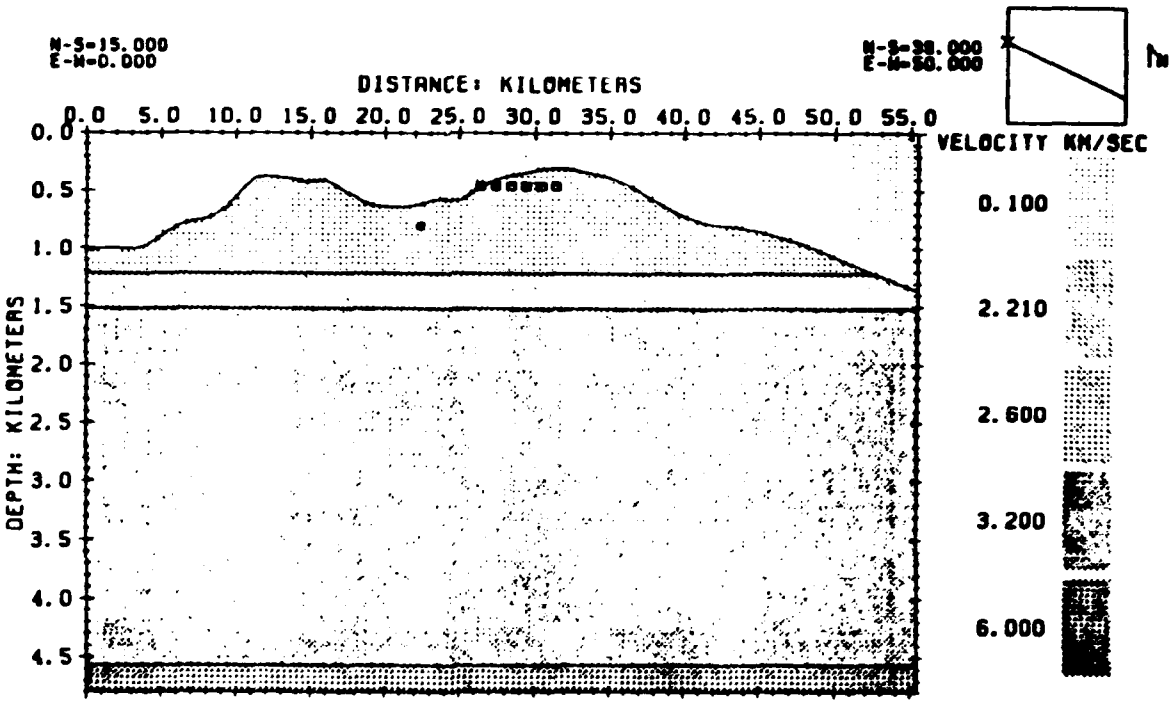

GENERIC MOUNTAIN WITH 4 VELOCITY LAYERS

FIGURE 6. Cross section of model 2 along profile C.

TABLE 2

SOURCE - RECEIVER GEOMETRY

	X (N-S) (km)	Y (E-W) (km)	Z (DEPTH) (km)	LAYER
Source	25.0	20.0	0.8	1

RECEIVER PROFILES AT Z (DEPTH) = 0.4572 km

Profile	AZIMUTH* (degrees)	DISTANCE TO 1st RECEIVER (km)	DISTANCE TO LAST RECEIVER (km)	RECEIVER SPACING (km)
A	338	5	10	1
B	67	3	10	1
C	116	5	10	1

RECEIVER ARRAYS AT Z (DEPTH) = 0.4572 km

ARRAY	STATION	X (N-S) (km)	Y (N-S) (km)	DISTANCE FROM SOURCE (km)	AZIMUTH (degrees)
A	1	16	16	9.85	336
A	2	16	17	9.49	342
A	3	17	16	8.94	333
A	4	17	17	8.54	339
B	1	22	25	5.83	59
B	2	22	26	6.71	63
B	3	23	25	5.39	68
B	4	23	26	6.32	72
C	1	28	27	7.62	113
C	2	28	28	8.54	111
C	3	29	27	8.06	119
C	4	29	28	8.94	117

*Source receiver azimuth measured clockwise from N.

A profile and one for the B and C profiles, with 1/2 the grid node spacing used in the low frequency calculation. The high and low frequencies for each receiver response were then merged. For each calculation, the model was sampled on a 128 x 128 grid, centered on the area of interest. The grid was smoothly tapered to a horizontal boundary on the edges and extended to 256 x 256 points for the calculation. The frequency range of the calculations were from 0 to 11 hz at an interval of 0.2 hz giving a 5 s time window for each response.

Tapering and padding the model suppressed only some of the wraparound and edge effects resulting from using the Finite Fourier Transform in the calculations. We are still faced with aliasing and wraparound effects that cannot be removed by simply increasing the size of the model. These result from the implicit spatial and temporal periodicity of the wavefield in the frequency domain using finite Fourier transforms: the source is assumed to be both periodic in time and located at regular intervals in space. The amplitude decay with distance between source and receiver that results from the wave equation cannot sufficiently attenuate arrivals from adjacent intervals and from sources other than the one of interest. The numerical techniques necessary to describe three dimensional wave propagation using Fast Fourier Transforms is described by Bouchon (1979) and is further discussed in Aki and Richards (1980). Essentially, the response is computed using a complex value for frequency, of which the imaginary part is assigned to suppress the amplitude of propagating waves with distance. After computing the time domain response, the effects of the complex frequency value can be removed for the time window of interest by multiplying by an exponentially increasing time function.

7.0 RAYTRACING AND BIE CALCULATIONS FOR AFGL MODEL

To check the results, we compared the profiles with results from Sierra's raytracing package QUIKSHOT^{TM}. The BIE formulation presented earlier makes these comparisons easy since we can effectively compute a ray expansion and explicitly include the same propagation paths modeled in the raytracing. To trace rays we used model 2 as described in the previous section and, again, simulated a fluid medium by making the S-wave velocity negligibly small. We designed the raytracing problem to be simple enough to easily interpret the results, yet complex enough so that complications due to three dimensional effects can be checked and compared. We compute what we will call the primary response, which includes all primary reflections from the subsurface layers as well as the direct wave. Because of the proximity of the source and receivers to the free surface we include all of the interaction with the free surface near both the source and the receivers. In all, 13 raypaths were deemed necessary to compute a "primary" solution; these are schematically given in Figure 7.

The comparison of the BIE and raytracing results are presented in Figures 8 and 9. The source function in all cases is a "Ricker" wavelet, shown in Figure 10, which is the second time derivative of a Gaussian pulse with a peak frequency response at 5.5 hz. We have plotted both pressure and the vertical component of displacement. There is some disagreement between the results at receivers 6, 7 and 8; note the larger relative amplitude of the second arrival. This is because the rays interacting with the lower layers go through the critical angle at these distances. The amplitudes of the raytracing results are least accurate near the critical angle. Overall, the agreement between the raytracing solution and the BIE solution is very good, providing confidence that the BIE calculations are working correctly. Conversely, it shows that ray tracing provides very useful results for some problems.

To compare the AFGL models, Model 1 and 2 from Generic Mountain B, we show the three profiles for the two models in Figures 11 to 16.

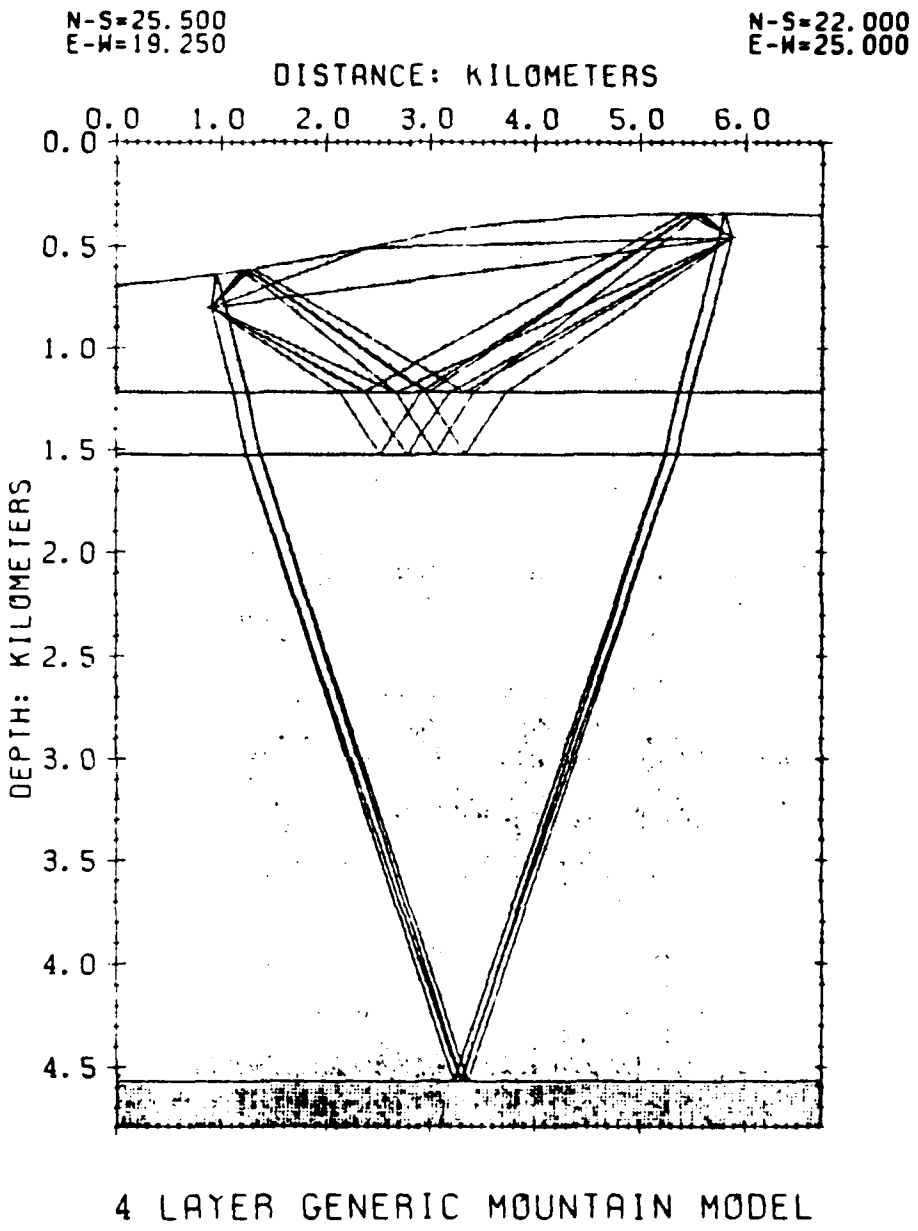

FIGURE 7. Raypaths used in raytracing calculations between the source and a single receiver. The rays also show conceptually the propagation and interactions used in the BIE calculations.

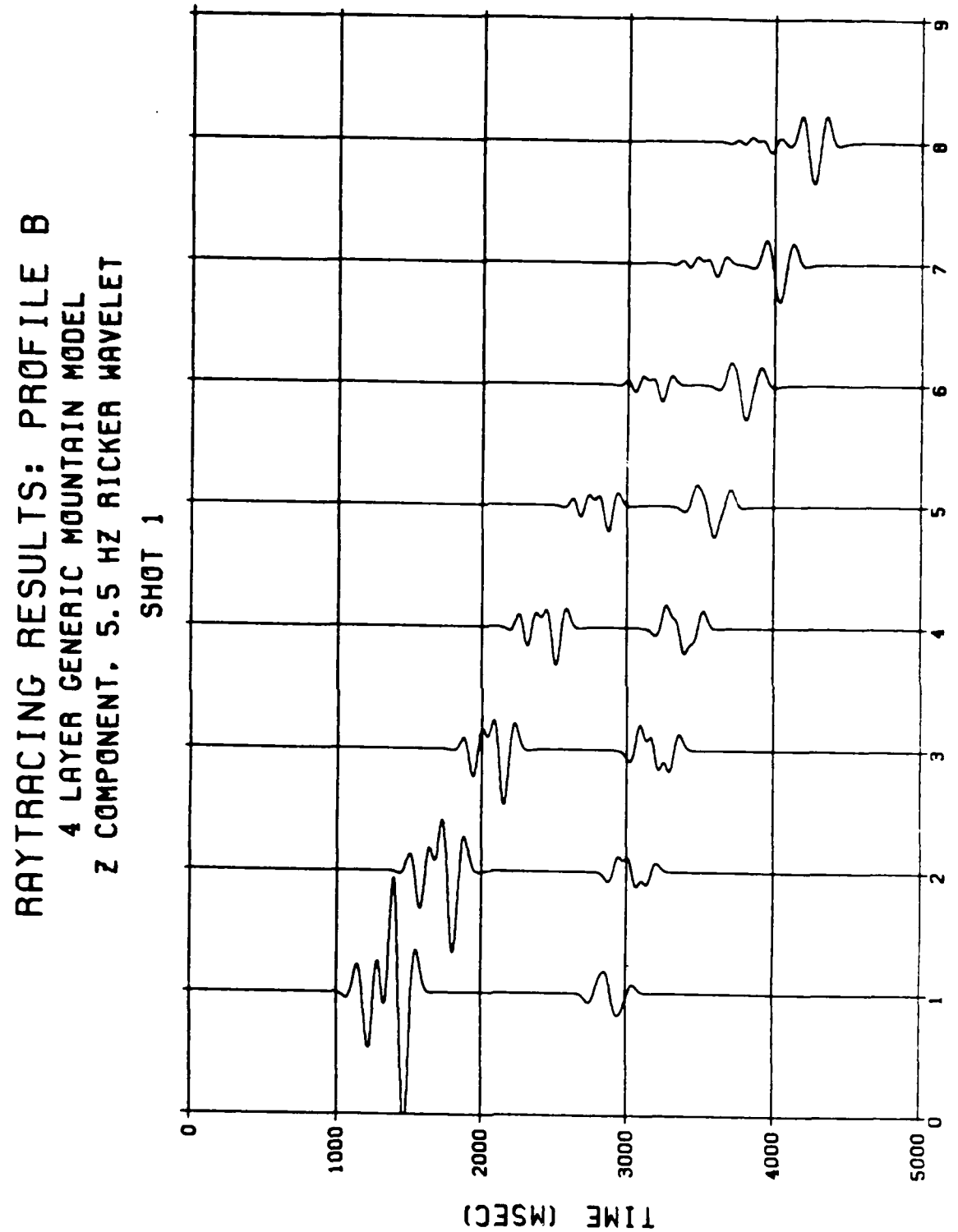

FIGURE 8.a. Comparison of vertical displacement component synthetic seismograms computed by raytracing (a) and the BIE method (b) for profile B. The source time function is a 5.5 hz Ricker wavelet as shown in Figure 10.

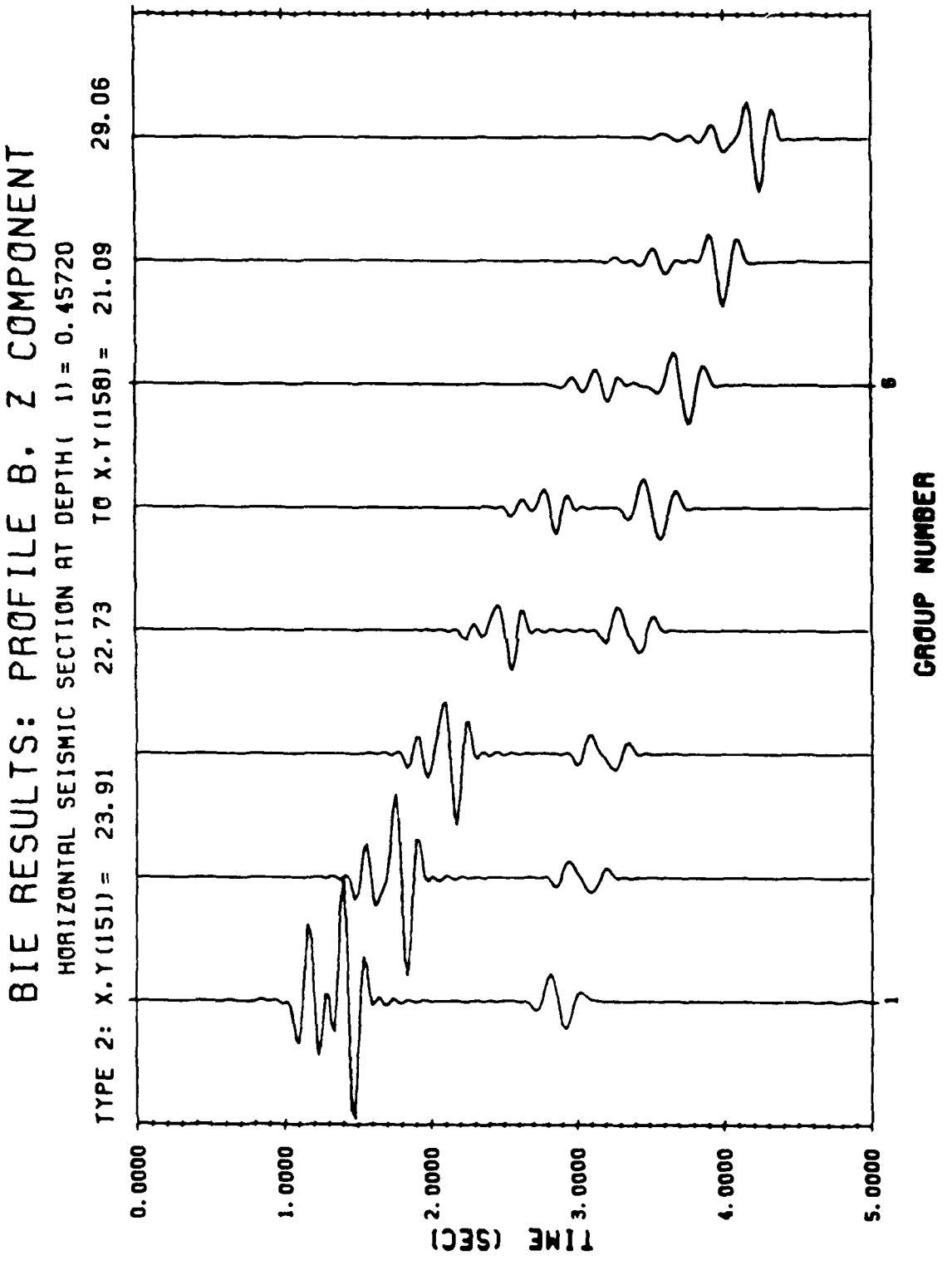
BIE RESULTS: PROFILE B, Z COMPONENT
HORIZONTAL SEISMIC SECTION AT DEPTH(1)= 0.45720
TYPE 2: X,Y(151)= 23.91 22.73 TO X,Y(158)= 21.09 29.06
0.0000
1.0000
2.0000
3.0000
4.0000
5.0000
TIME (SEC)
1
6
GROUP NUMBER

FIGURE 8.b.

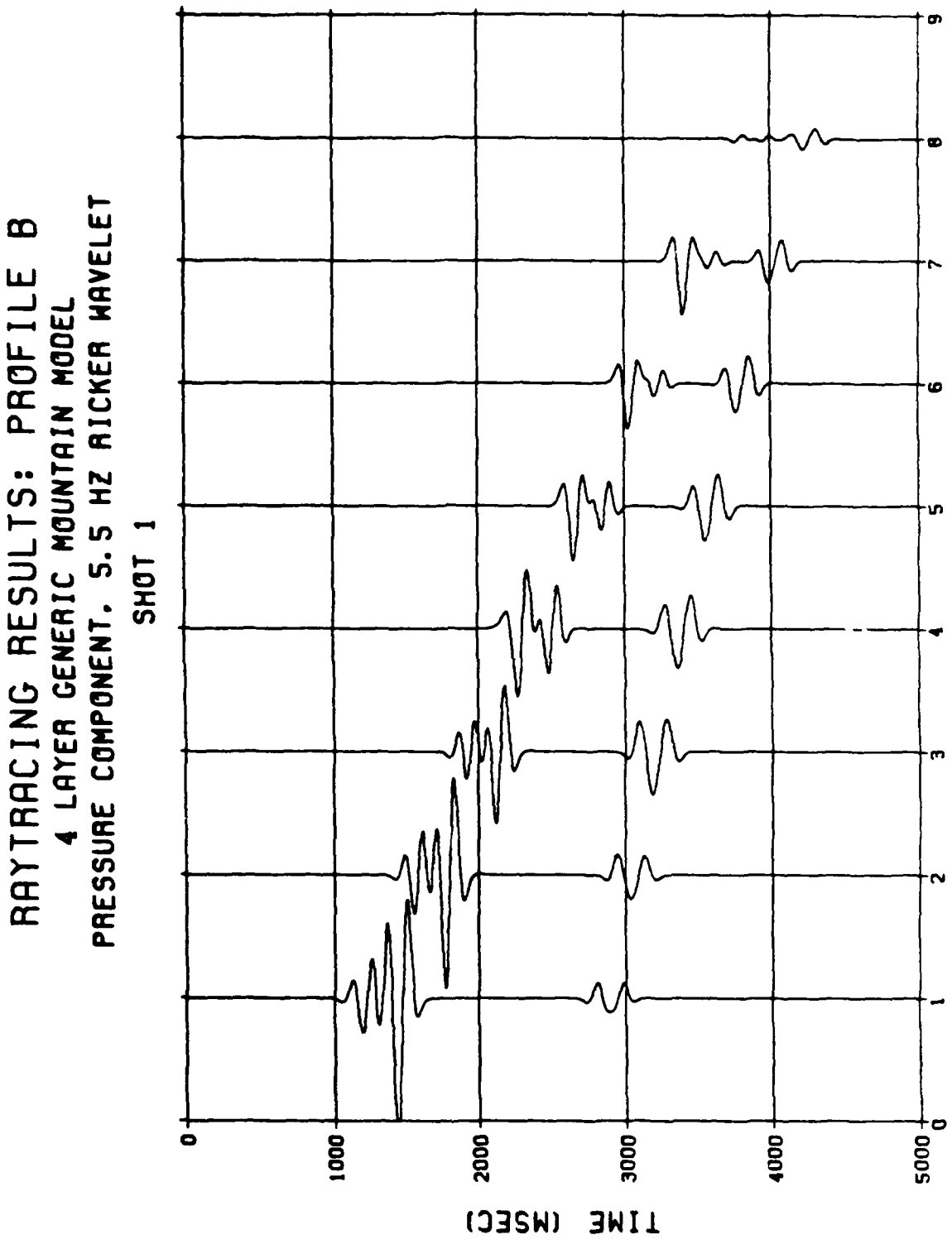

FIGURE 9.a. Comparison of pressure component synthetic seismograms computed by (a) raytracing and (b) the BIE method for profile B.

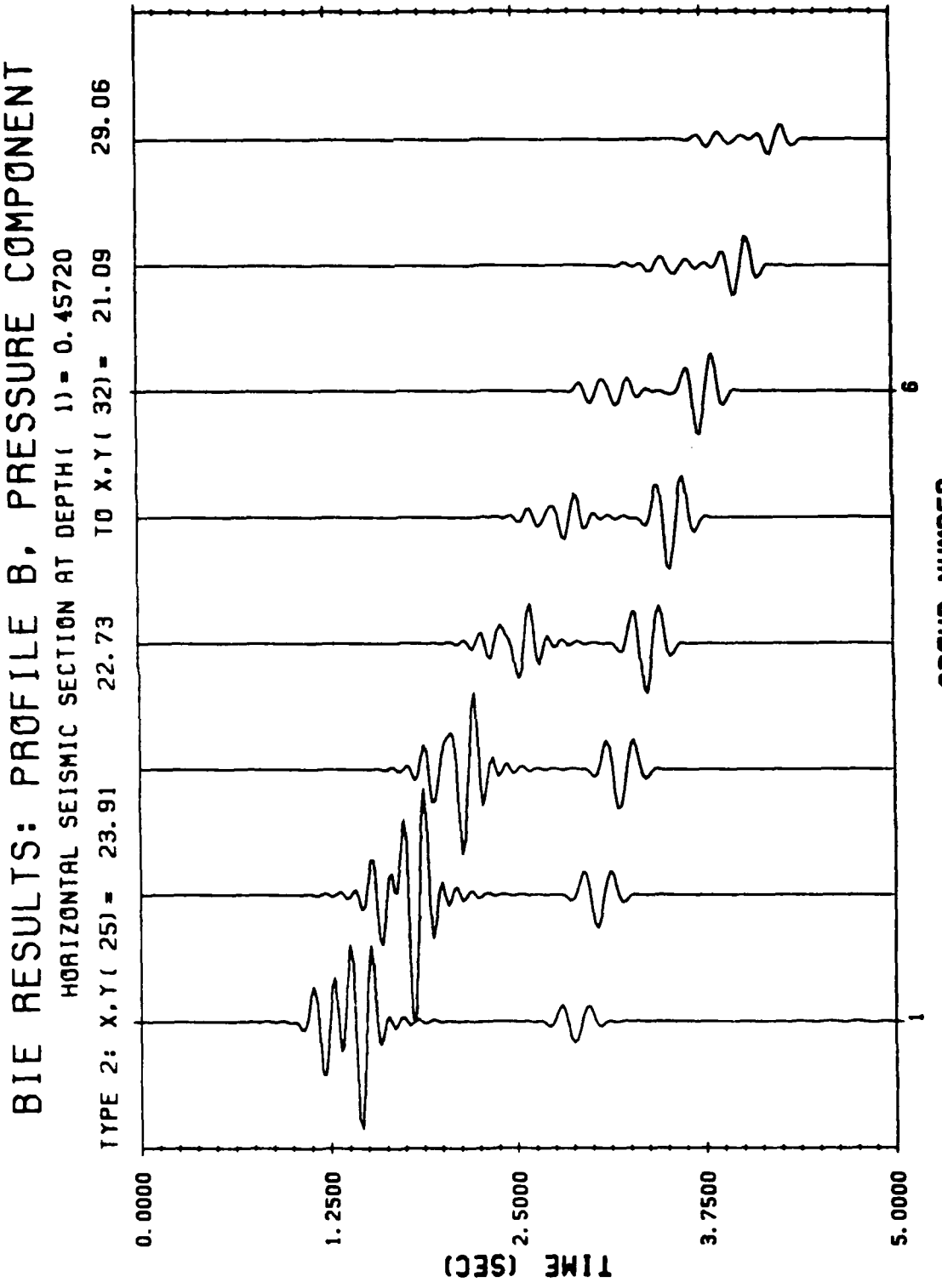
BIE RESULTS: PROFILE B, PRESSURE COMPONENT
HORIZONTAL SEISMIC SECTION AT DEPTH(1) = 0.45720
TYPE 2: X,Y(25) = 23.91 22.73 TO X,Y(32) = 21.09 29.06
0.0000
1.2500
2.5000
3.7500
5.0000
TIME (SEC)
GROUP NUMBER
1
6

FIGURE 9.b.

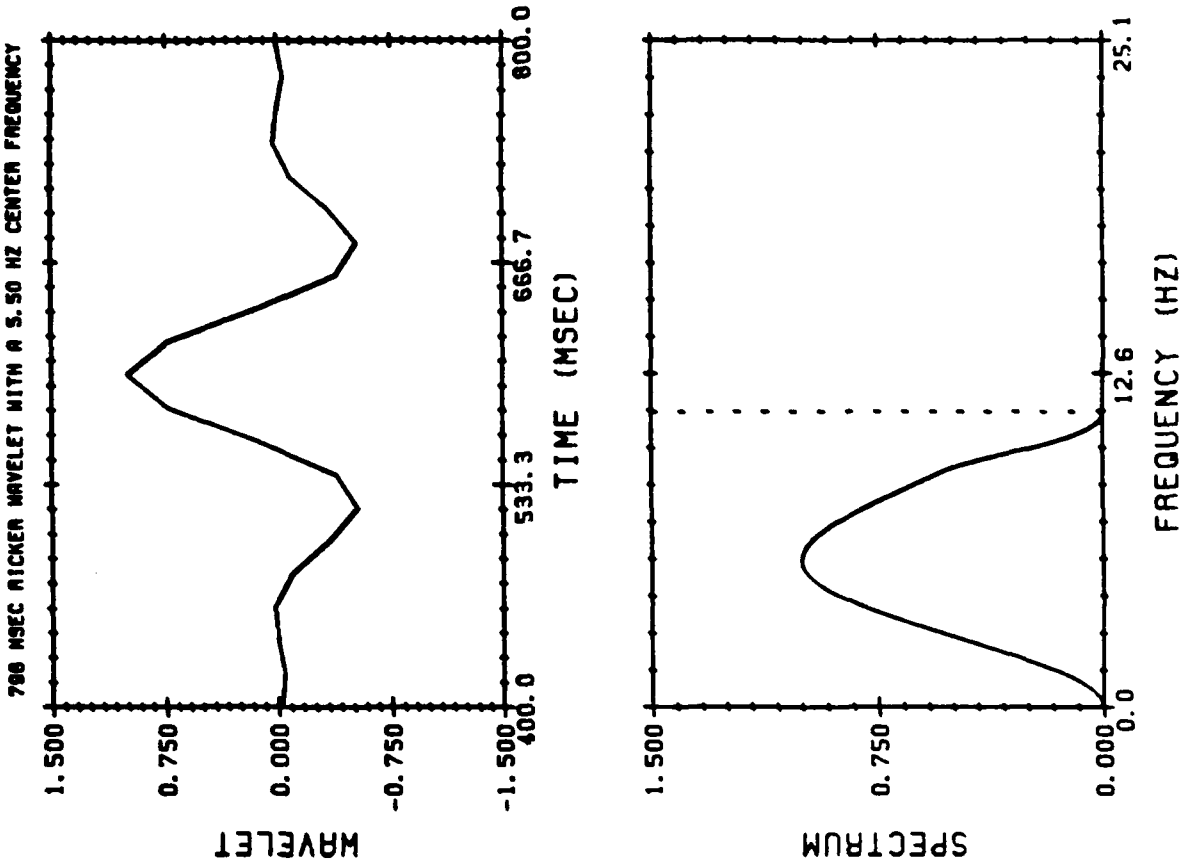

FIGURE 10. A 5.5 hz Ricker wavelet.

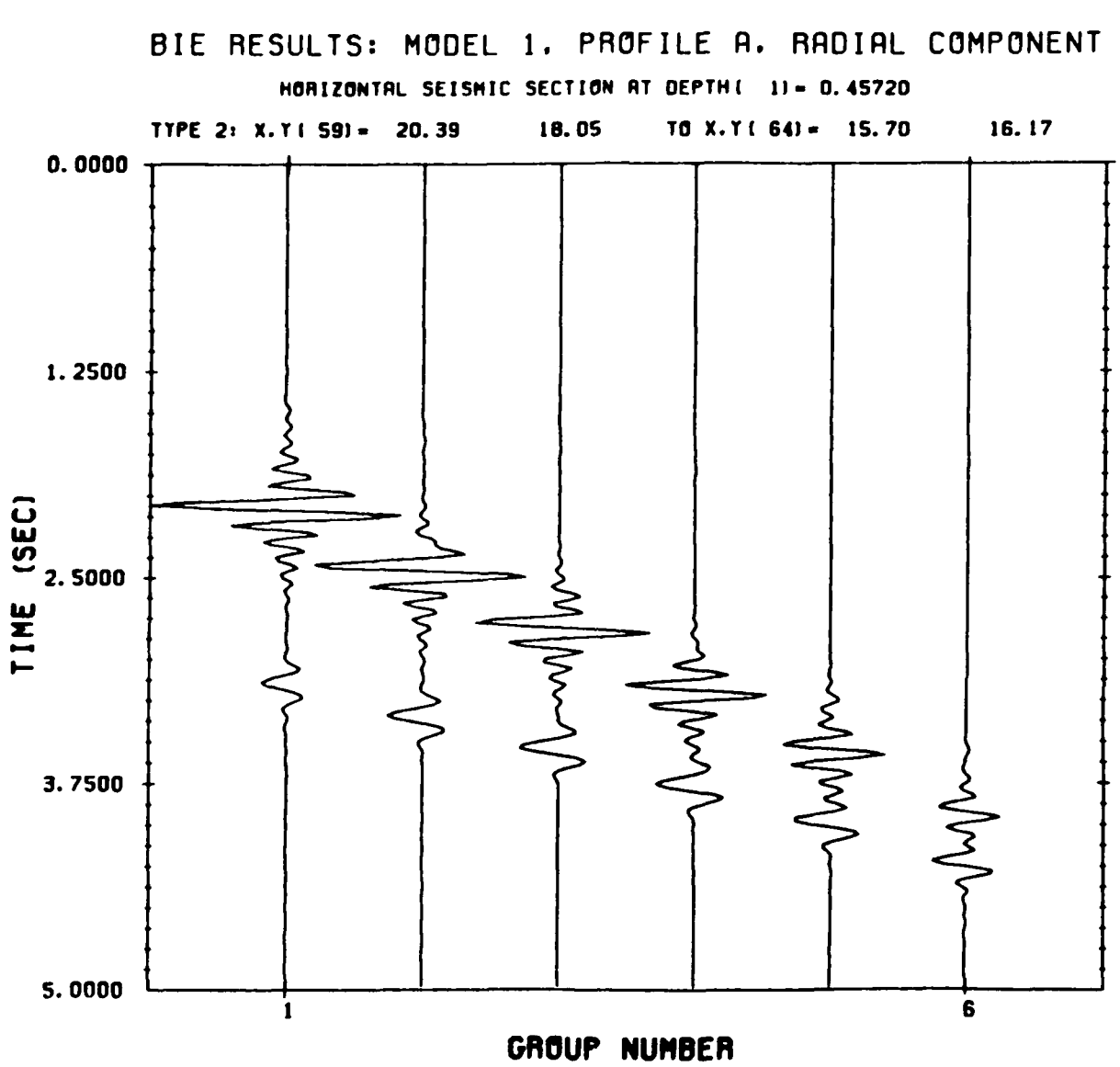

FIGURE 11. The radial component of the displacement response for model 1, profile A, calculated by the BIE method for primary reflections only. The source is a step function of 1-N-m amplitude. The response has been tapered between 8.8 and 11 hz, otherwise no wavelet has been applied. Traces are scaled to a peak amplitude of 6.02×10^{-14} m for trace 1.

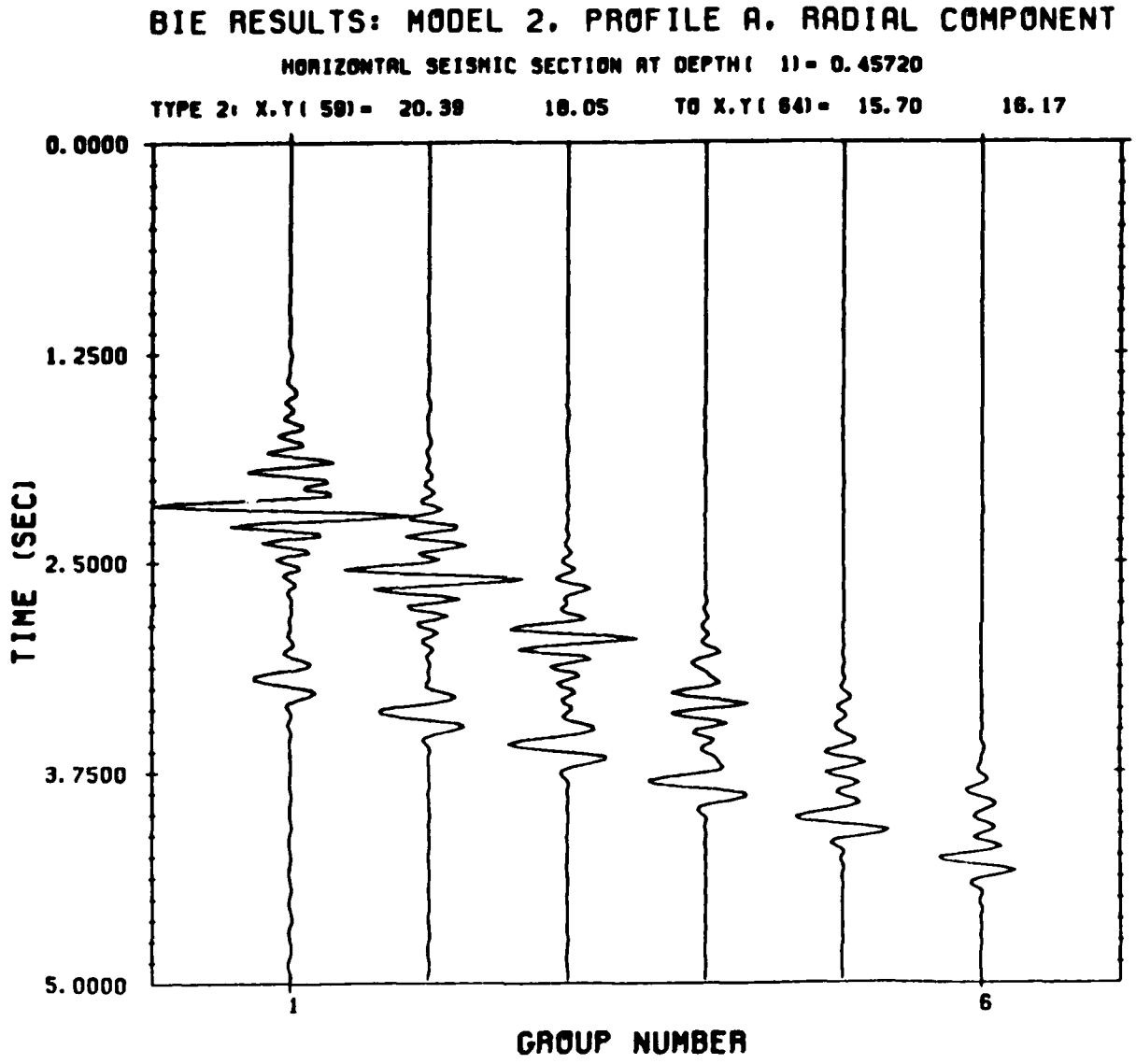

FIGURE 12. The radial component of the displacement response for model 2, profile A, calculated by the BIE method for primary reflections only. The traces are scaled to a peak amplitude of 3.63×10^{-14}m for trace 1.

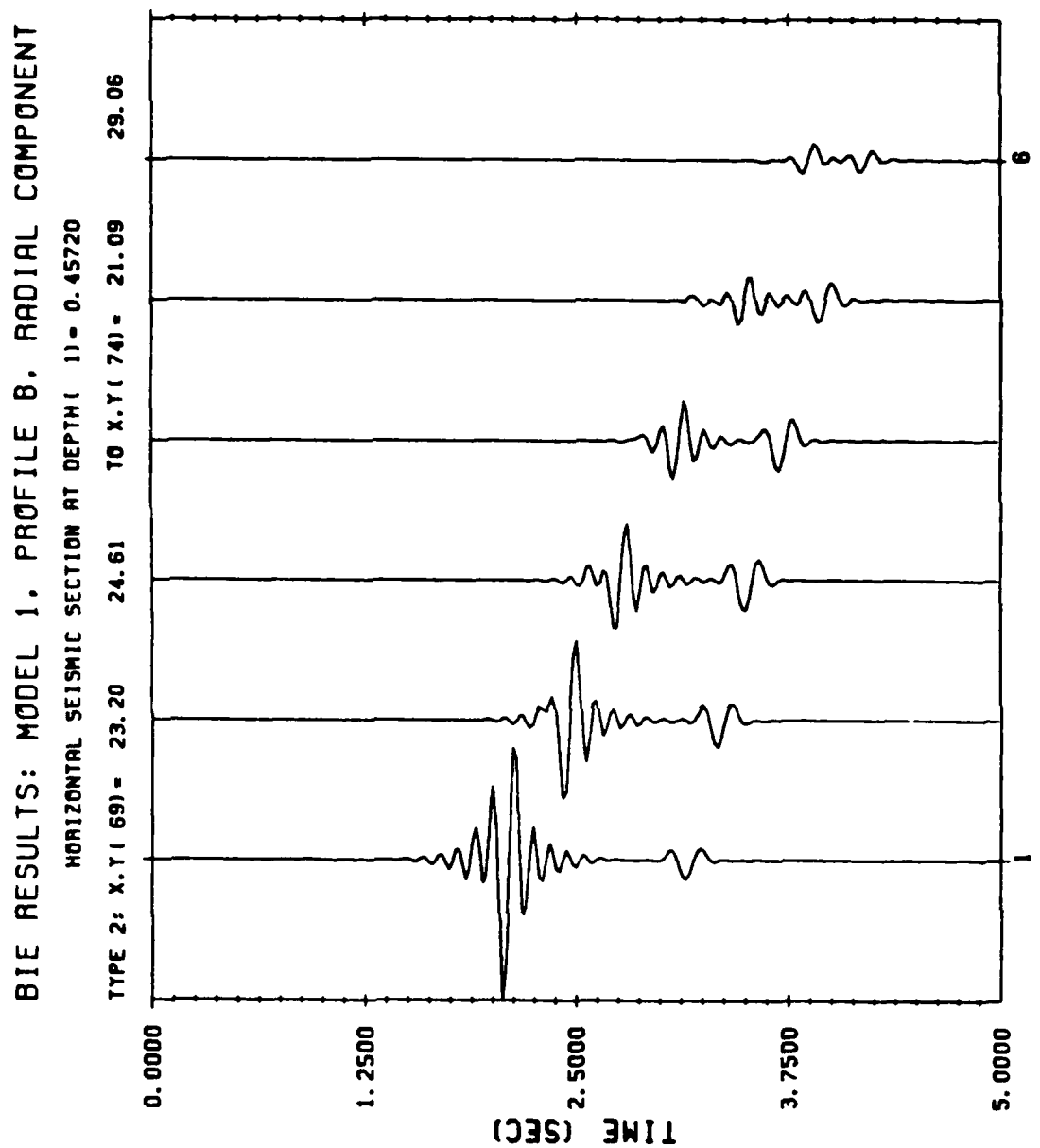

FIGURE 13. The radial component of the displacement response for model 1, profile B, calculated by the BIE method for primary reflections only. The traces are scaled to a peak amplitude of 7.14×10^{-14} m for trace 1.

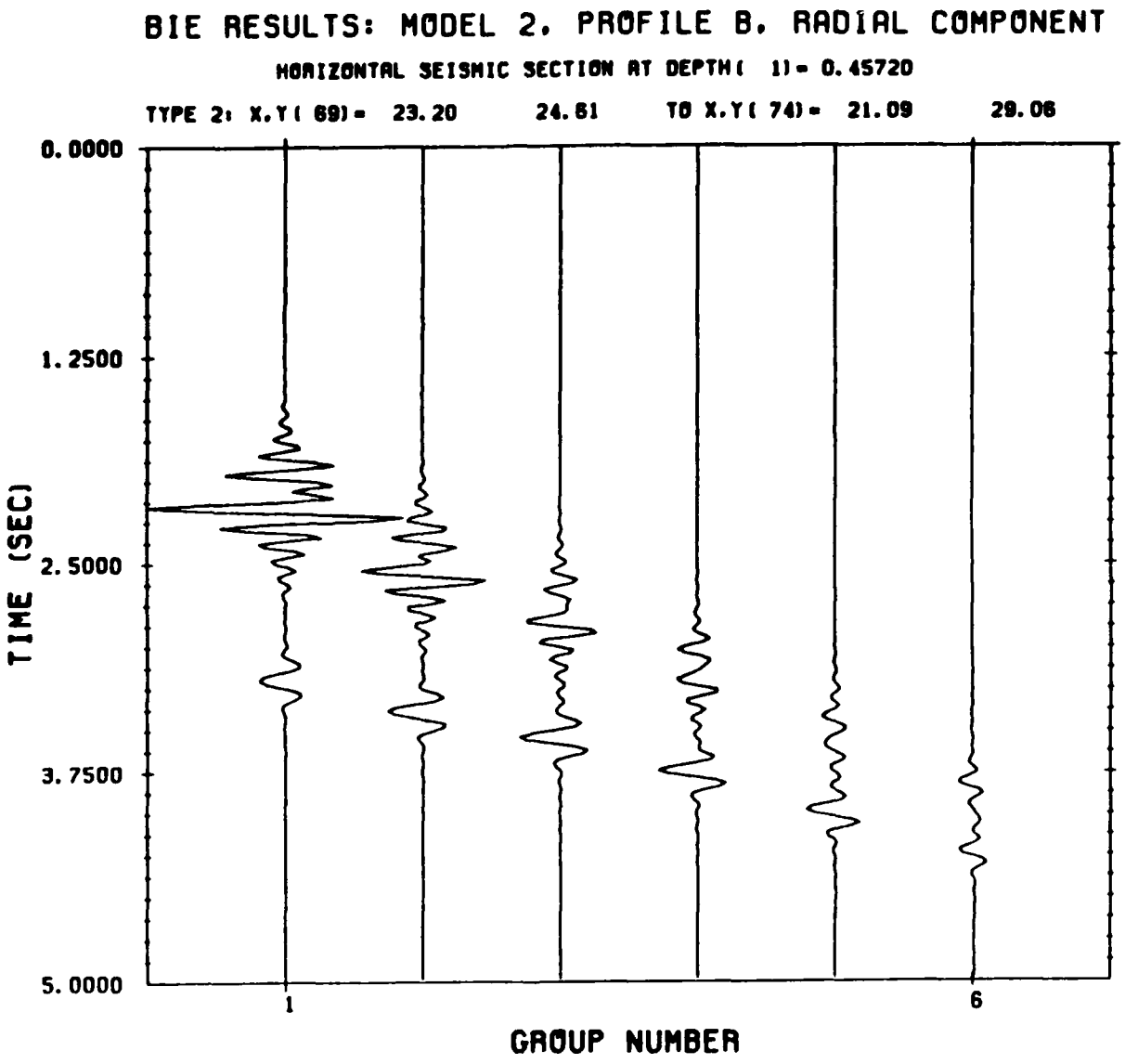

FIGURE 14. The radial component of the displacement response for model 2, profile B, calculated by the BIE method for primary reflections only. The traces are scaled to a peak amplitude of 4.95×10^{-14}m for trace 1.

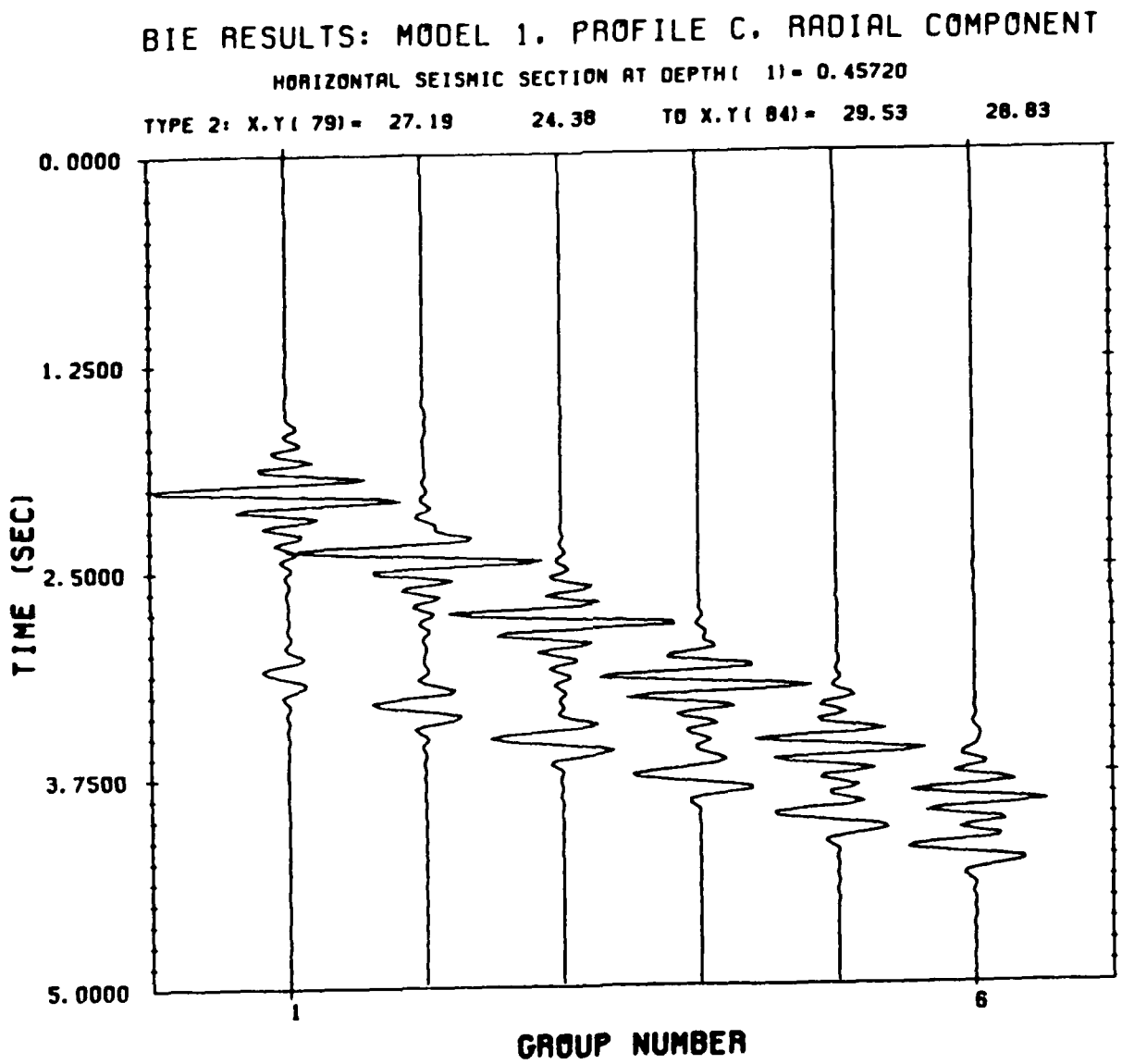

FIGURE 15. The radial component of the displacement response for model 1, profile C, calculated by the BIE method for primary reflections only. The traces are scaled to a peak amplitude of 3.36×10^{-14}m for trace 2.

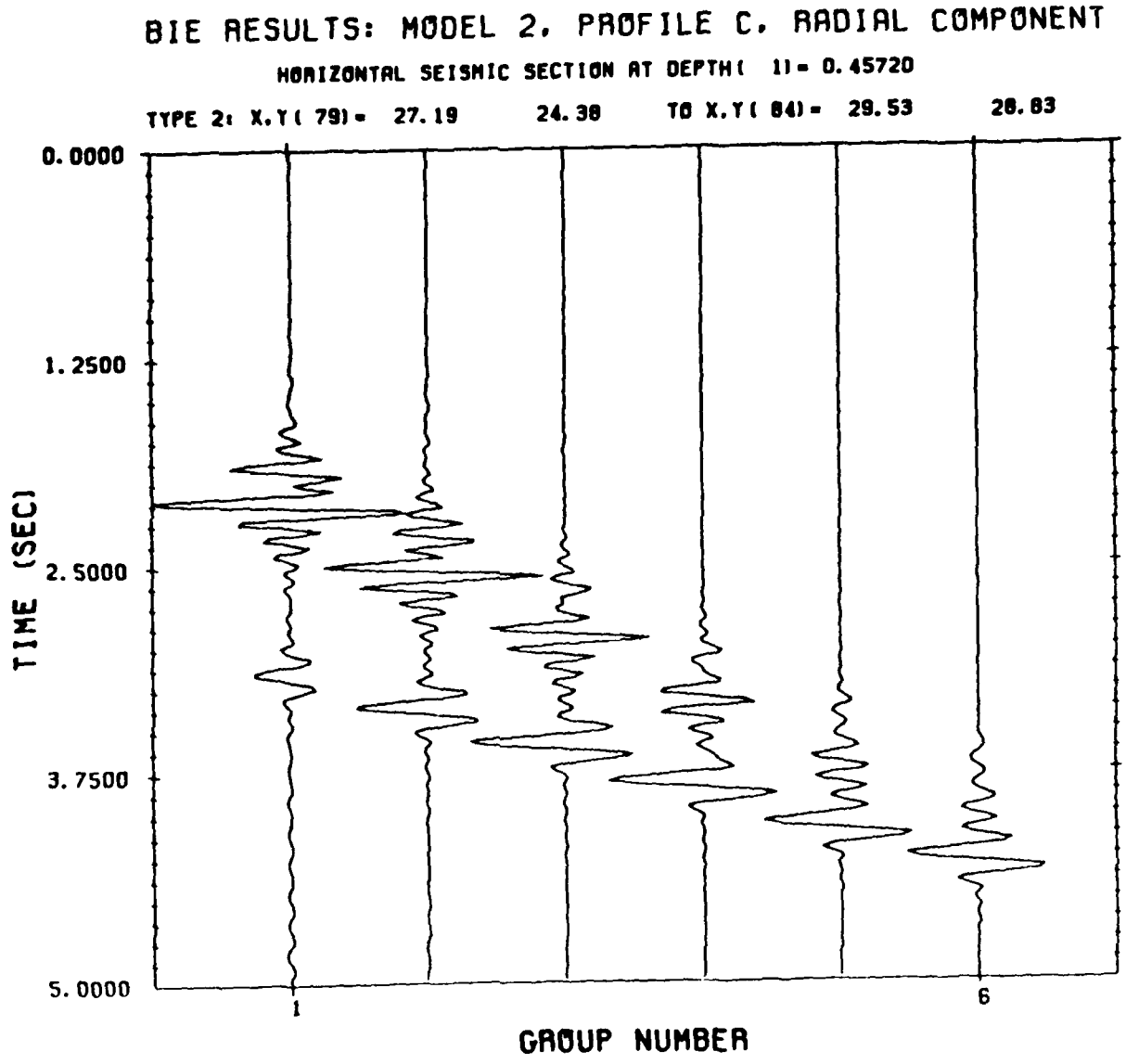

FIGURE 16. The radial component of the displacement response for model 2, profile C, calculated by the BIE method for primary reflections only. The traces are scaled to a peak amplitude of 2.32×10^{-14}m for trace 1.

These calculations were made for the primary response, which considers only those raypaths (or energy paths) diagrammed in Figure 7. In all cases we give the radial component of displacement, since, for the geometry under consideration, this will be the dominant component of motion. The amplitudes are scaled to a pressure source with a step function time history of 1 N-m amplitude. The seismograms have been low-pass filtered with a frequency taper between 8.8 and 11 hz. Each profile extends from about 5 to 10 km; the plane of the receivers (at Z = 0.4572 km) intersected the free surface near 4 km along profiles A and C. Therefore, the closest receiver located below the surface of the mountain was beyond the distance where critical reflection from the 3.2 km interface occurs for both models (this critical distance is 2.5 km for model 1 and 2.2 km for model 2).

The difference between the two models (i.e., the low velocity zone) shows up in differences in the peak amplitude of the first arrivals. In model 1 the first arrival is an interference of the direct ray, head wave from the 3.2 km interface, the post-critical reflection from the 3.2 km interface and all of the associated interactions with the free surface. These arrivals are all within 0.12 s. The firs large arrival on all of the model 1 profiles is the result of the interference of the direct wave and the post critical reflection from the 3.2 km interface. A small head wave from the 3.2 km/s layer becomes evident at farther ranges. In model 2, the direct wave arrives almost 0.2 s before the post critical reflection from the 3.2 km/s layer, which results in a more dispersed group of first arrivals with lower peak amplitudes than for model 1. In both models the amplitude of the later reflection from the 6 km/s interface is similar; this arrival has a critical distance of about 8 km.

While the difference in peak amplitudes between models 1 and 2 can be explained by the presence of the low velocity zone, the difference in amplitudes among the three profiles may be explained by the structure of the free surface. One large difference is at the near distance range of 5 and 6 km: profile C shows markedly smaller peak amplitudes than profiles A and B, which are similar. Reference to Figures 3, 4, 5 and 6 show that two effects are likely important. First, for profiles A and

C, the receiver at 5 km distance is in a "shadow" for the direct wave, i.e. a ray from the source to the 5 km receiver intersects the free surface, which reduces the amplitude of the direct arrival. This effect likely explains the slight amplitude differences between profiles A and B. Second, profiles A and B encounter largely two-dimensional structure (see Figure 3) for the wavelengths of interest; in other words, the energy propagates along the same direction as the major variations in the structure. The free surface interaction along profile C is more three dimensional, the structure varying obliquely to the direction of wave propagation, and energy is scattered out of the plane of propagation, significantly reducing the amplitudes at the near ranges.

The amplitude pattern among the profiles changes at the more distant ranges (9-10 km) where profile B shows peak amplitudes less than 1/2 those of profile A and C. The reason is similar to that discussed above. Profiles A and C are encountering two-dimensional structure at these ranges while profile B encounters three dimensional structure that causes significant out-of-plane scattering in the free surface interaction.

Consideration of the more familiar wave propagation phenomena in plane layered media indicates that at the distance ranges of interest in this study, the primary reflections are not the dominant contribution to the seismogram. The distances are well beyond critical, and the source is located in a low velocity layer, which means that considerable energy is propagating as trapped waves in the near surface layers. In our acoustic model, these trapped waves are analogous to the Love waves in elastic models for the earth. To model these waves the calculations must account for several interactions between the lower layers and the free surface, requiring considerably more computer effort. The convergence of the ray expansion has been considered by several authors (e.g. Hron, 1971); we simply argue that, since 10 km is approximately 3 times the critical distance, we can reasonably expect to model these waves by considering up to three reflections from the lower layers.

We performed the more complete calculations only for Model 2 because of the effort involved. Large differences between the two results are not expected, and, given the level of approximation involved by neglecting many important elastic effects (such as Rayleigh waves), it is not expected that meaningful comparisons between the two models would result. Figures 17 through 19 show the radial displacement components for the three profiles for Model 2. In all instances the trapped waves dominate the responses; there is very little amplitude decay with distance. Now it is profile B that shows consistently larger amplitudes out to a distance of 9 km. Again, the waveforms for profiles A and C are remarkably alike, although the amplitudes on the near traces are about 25% larger on profile A. The three dimensional structure between the source and the near receivers on profile C is likely causing the reduced amplitudes; the similarity in waveforms between A and C is remarkable in view of the very different waveforms for profile B.

From the profiles presented in Figures 17-19 we see that interpreting trapped waves, or equivalently, surface waves that have propagated through arbitrary three-dimensional structures will be difficult. More modeling studies will be necessary to determine data analysis techniques that can map observable features onto structural parameters. Faster computers and improved algorithms for quickly calculating partial solutions are essential for learning how to interpret and predict three-dimensional wave propagation effects.

To verify the completeness of the solution within the context of an acoustic model, we computed complete synthetics using a wavenumber integration method (VESPA^{TM}) developed by Apsel (1979) for a flat-layered acoustic approximation to Model 2. The model was modified so that the free surface was at a depth of 0.4 km, with the source, receivers, and deeper structure unchanged. The results are shown in Figure 20. Although a seismogram by seismogram comparison is not very revealing, many of the features in the profiles computed by the BIE method are found in the VESPA solution. In particular, the approximate, relative decay of amplitudes is similar, as well as the duration of the high amplitude portions of the seismograms.

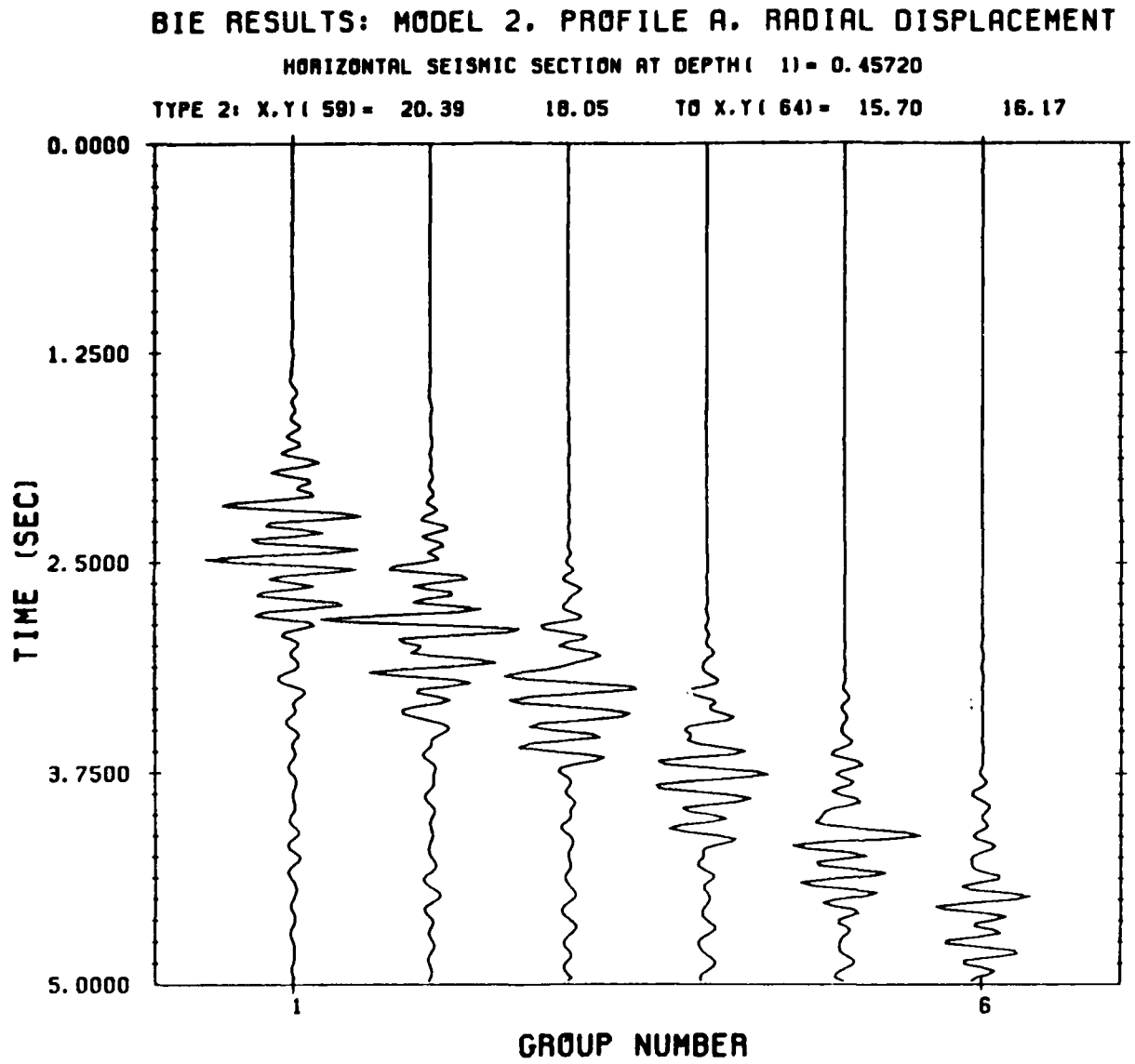

FIGURE 17. The radial component of the displacement response for model 2, profile A calculated by the BIE method including multiples up to third order (three reflections from the lower layers). The source amplitude is 1 N-m. The traces are scaled to a peak amplitude of 4.33 x 10^{-14} for trace 2.

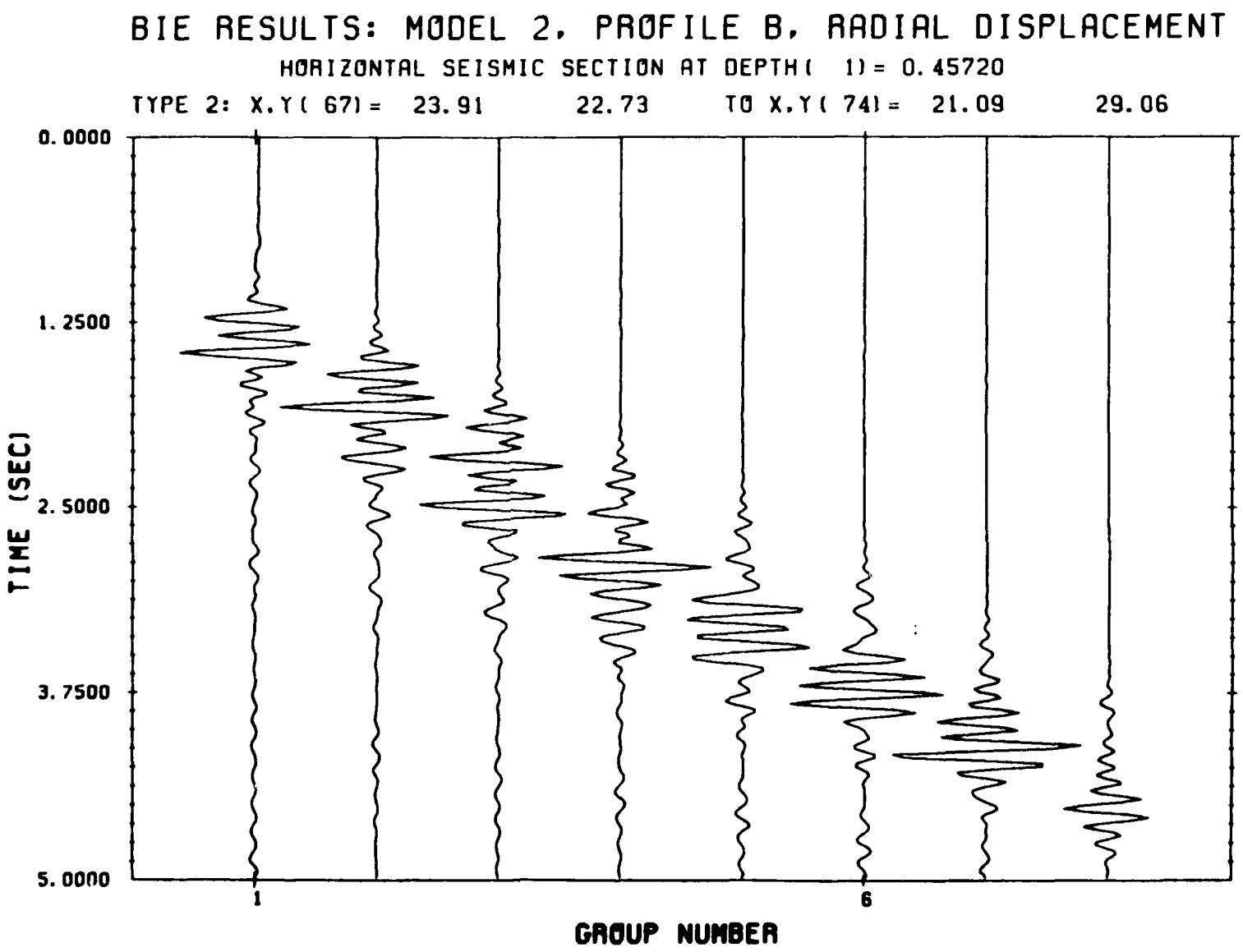

FIGURE 18. The radial component of the displacement response for model 2, profile B calculated by the BIE method including multiples to third order. The traces are scaled to a peak amplitude of 5.29 x 10^{-14}m for trace 2.

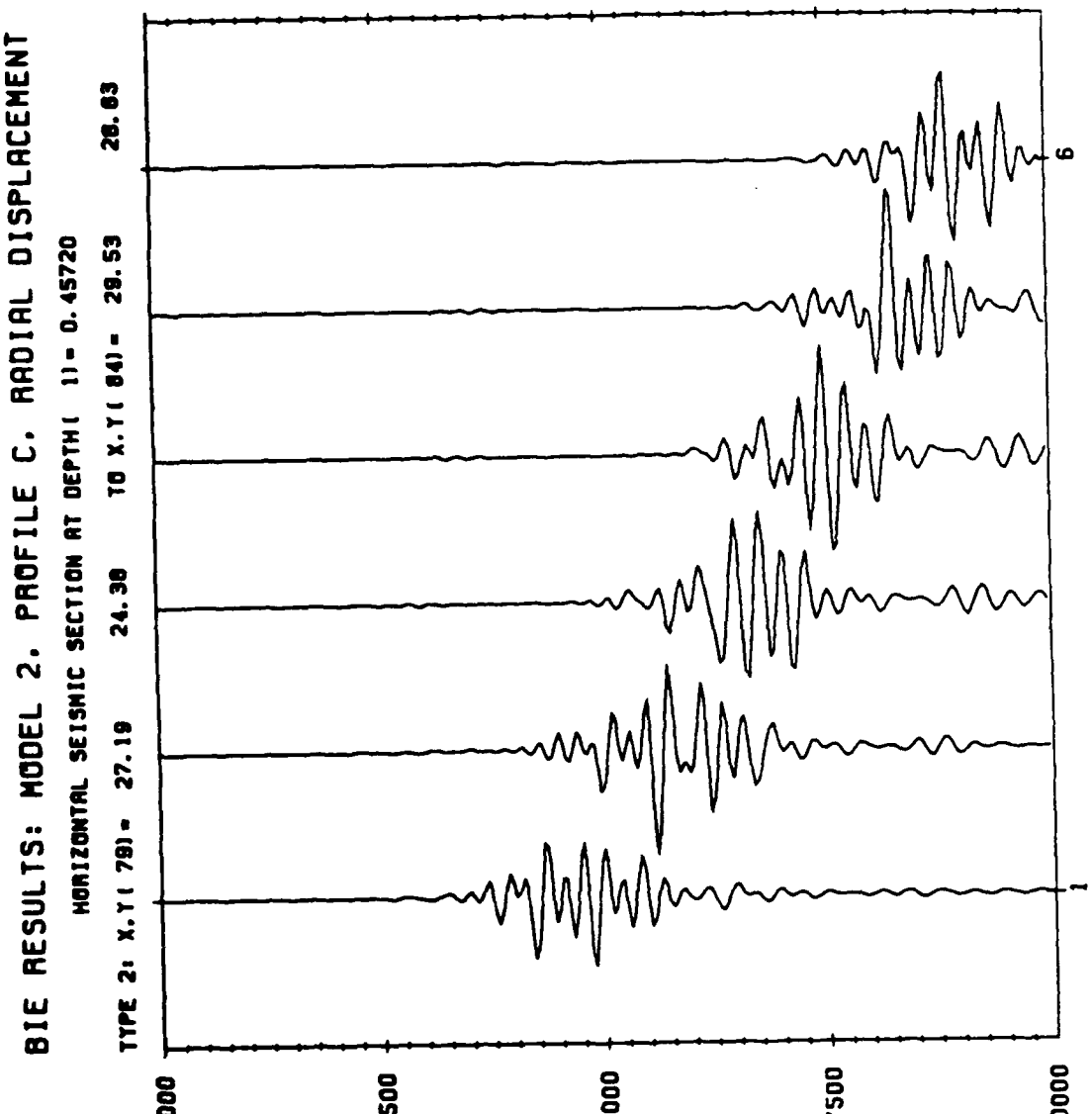

FIGURE 19. The radial component of the displacement response for model 2, profile C calculated by the BIE method including multiples to third order. The traces are scaled to a peak amplitude of 3.06 x 10^{-14}m for trace 2.

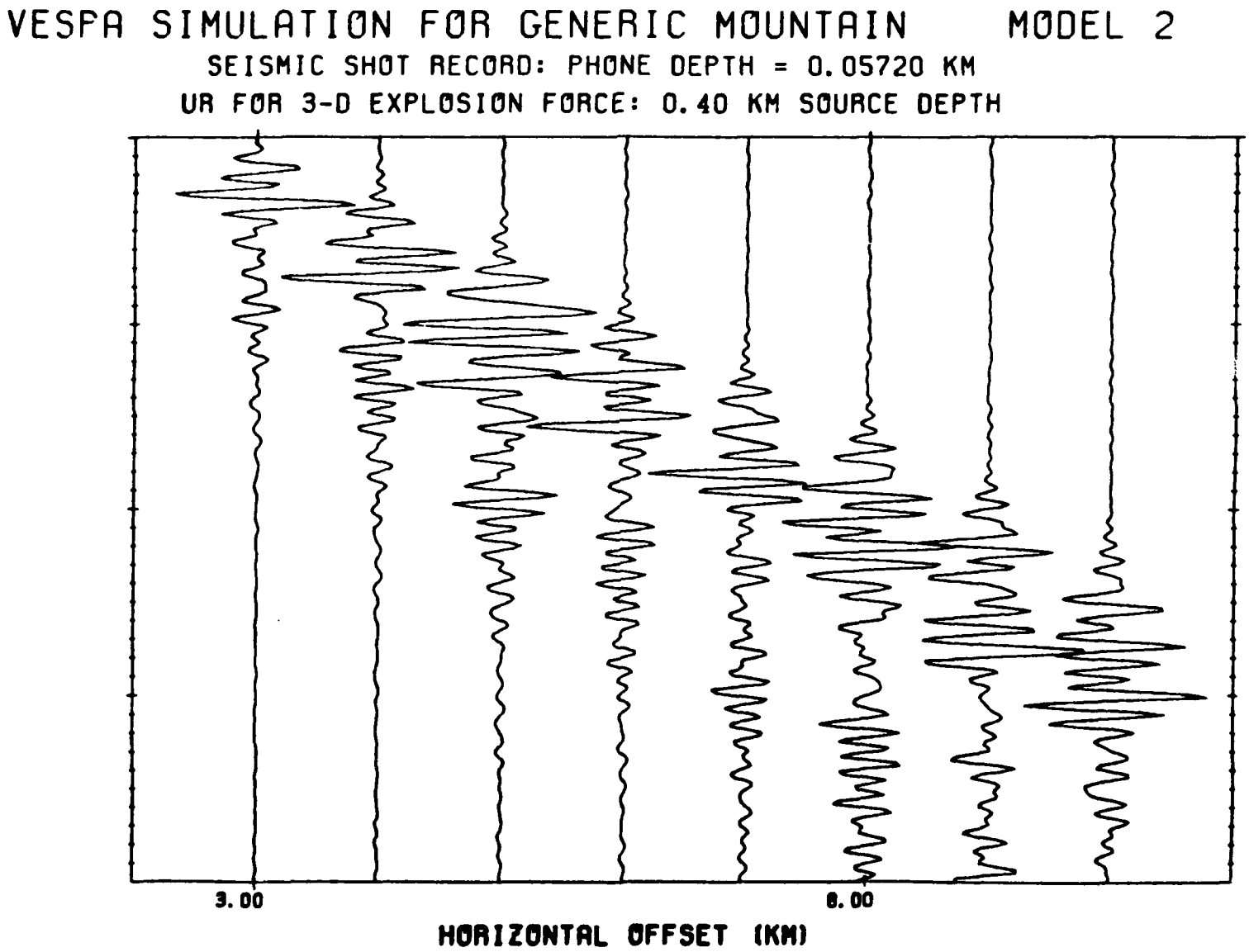

FIGURE 20. The radial component of displacement for a flat layered model calculated using a wavenumber integration method (Apsel, 1979).

We present the calculations for each of the three receiver arrays for both the primary and extended response calculated for Model 2. The traces have been convolved with a Ricker wavelet, peaked at 5.5 hz, to simulate the source spectrum as suggested by AFGL; the wavelet and its spectrum are shown in Figure 10. Figure 21 through 23 show the vertical and radial primary responses for the three arrays. Table 2 gives the array locations. The variations, within the arrays, of the relative amplitudes and the waveforms are slight indicating that the primary response is stable over 1 km distances. There is some amplification at station B-3 over what would be expected from normal decay with distance from the source. Array B shows the largest peak amplitude variation, only part of which is due to source-receiver distance.

The amplitude and waveform stability of the primary response is in contrast to the variations observed in the extended response. Figures 24-26 give the radial and vertical displacement response, including multiples up to the third order, for each array. Now peak amplitude variations of a factor of 2 between stations become evident for arrays A and C. This variation is larger than that associated with normal decay of amplitude with distance as can be seen by examining Figure 20. The amplitude variations are the result of subtle differences in the way the multiple responses combine. There is no obvious way to predict these amplitude variations short of modeling; it is very difficult to explain the behavior in the modeling results in terms of simple wave phenomena.

For the frequencies and wavelengths considered here, (<10 Hz, >0.25 km) the effects of surface topography on the amplitude and duration of strong shaking is not large compared to typical uncertainties in seismology arising from unknown velocity structure. Given these unknowns, the amplitude prediction from a flat layered wave-number integration method or even a generalized ray method are adequate. Given the dominance of the waveguide effects, either of these methods will be much more satisfactory than simple ray tracing.

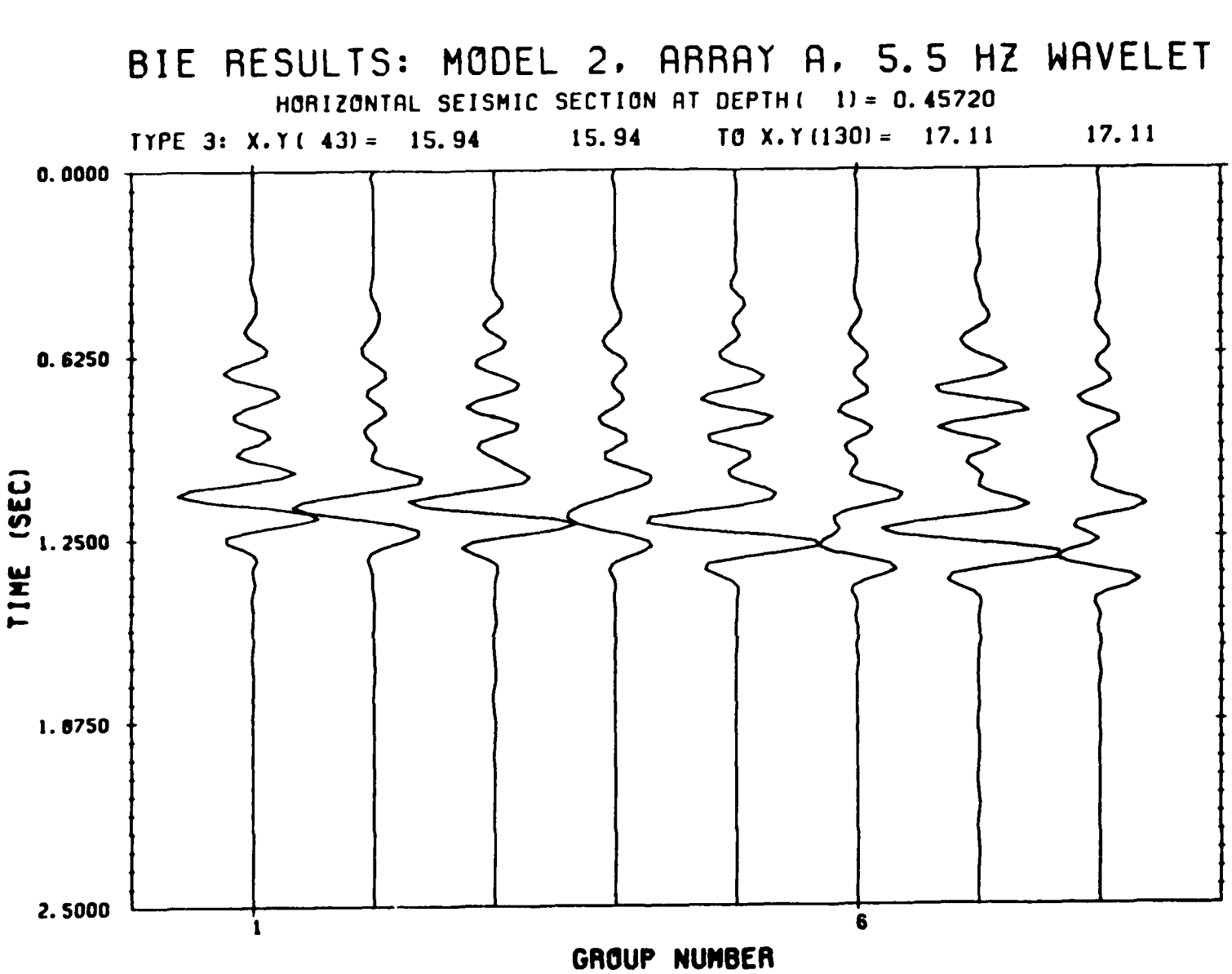

FIGURE 21. The radial and vertical components of displacement response for model 2, array A calculated by the BIE method using primaries only. A 5.5 hz Ricker wavelet (Figure 10) has been convolved with the response to a pressure source of 1 N-m. The order of stations is A-1 through A-4 with alternating radial and vertical components with radial first. The time scale is reduced using a velocity of 3.2 km/s. The traces are scaled to a maximum amplitude of 7.92×10^{-16}m on trace 5 (station A-3, radial).

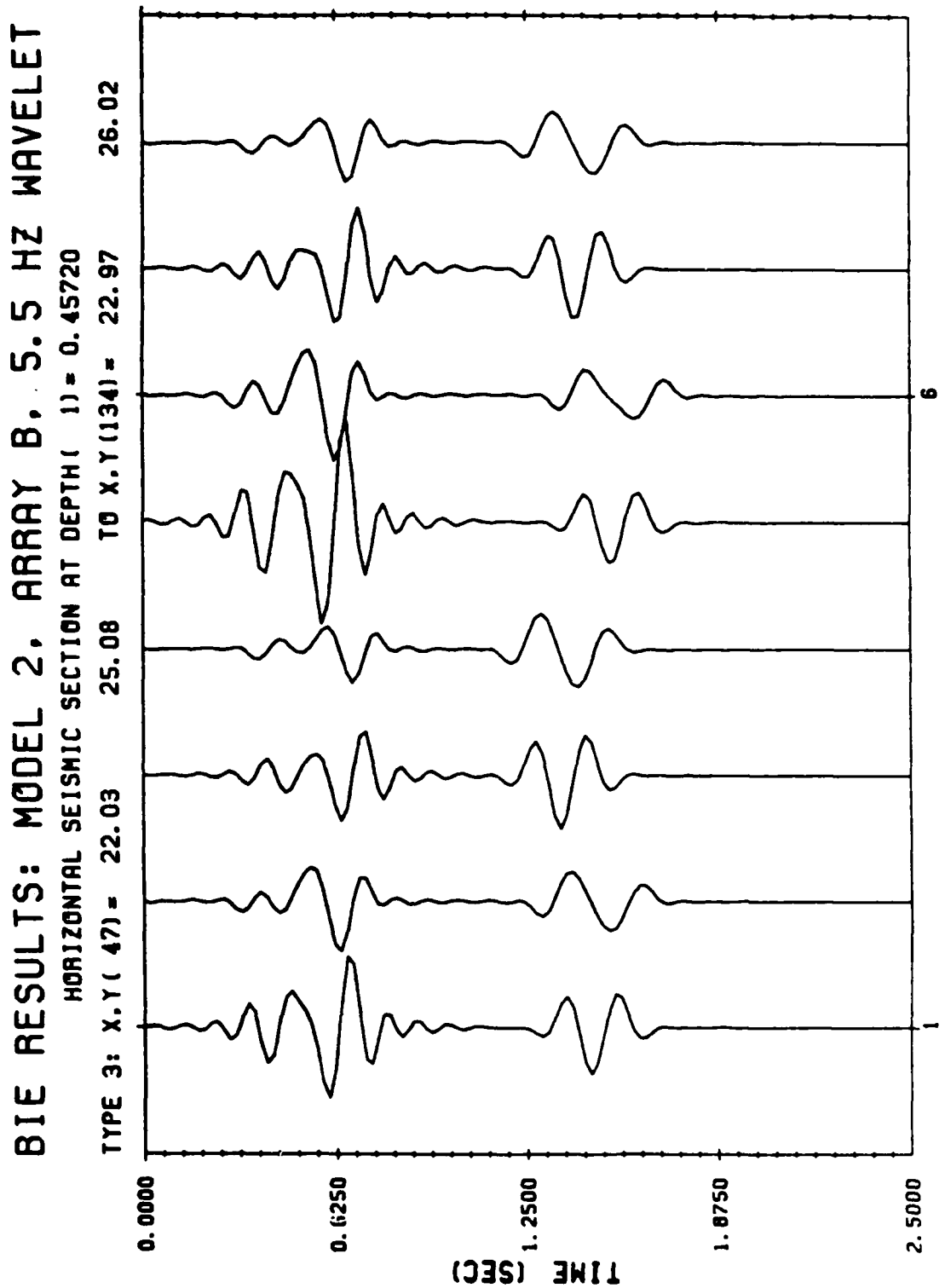

FIGURE 22. The radial and vertical components of displacement response for model 2, profile B calculated by the BIE method using primaries only. See caption, Figure 21. The traces are scaled to a maximum amplitude of 1.67×10^{-15} m on trace 5 (station B-3, radial).

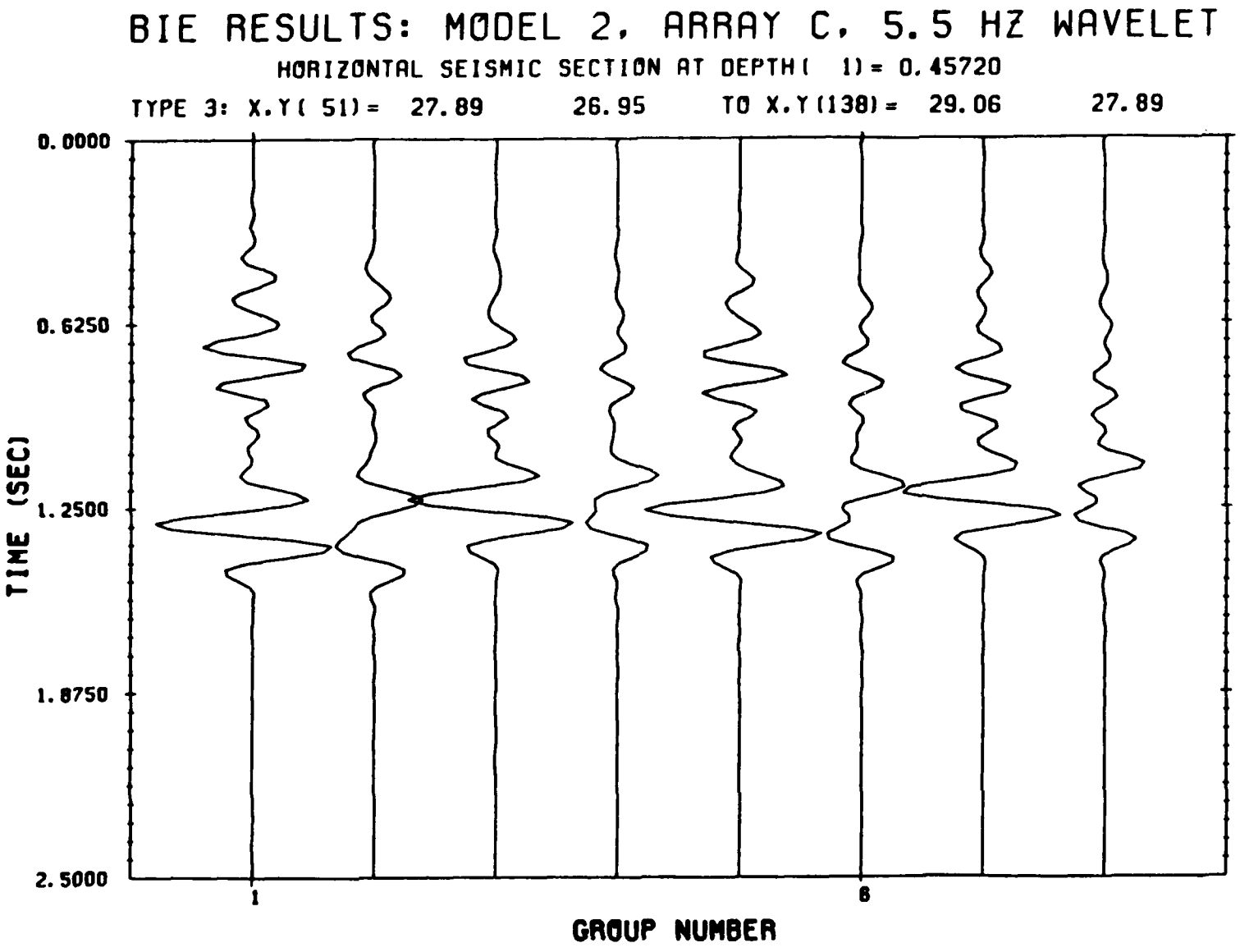

FIGURE 23. The radial and vertical components of displacement response for model 2, profile C calculated by the BIE method using primaries only. See caption, Figure 21. The traces are scaled to a maximum amplitude of 9.96×10^{-16}m on trace 1 (station C-1, radial).

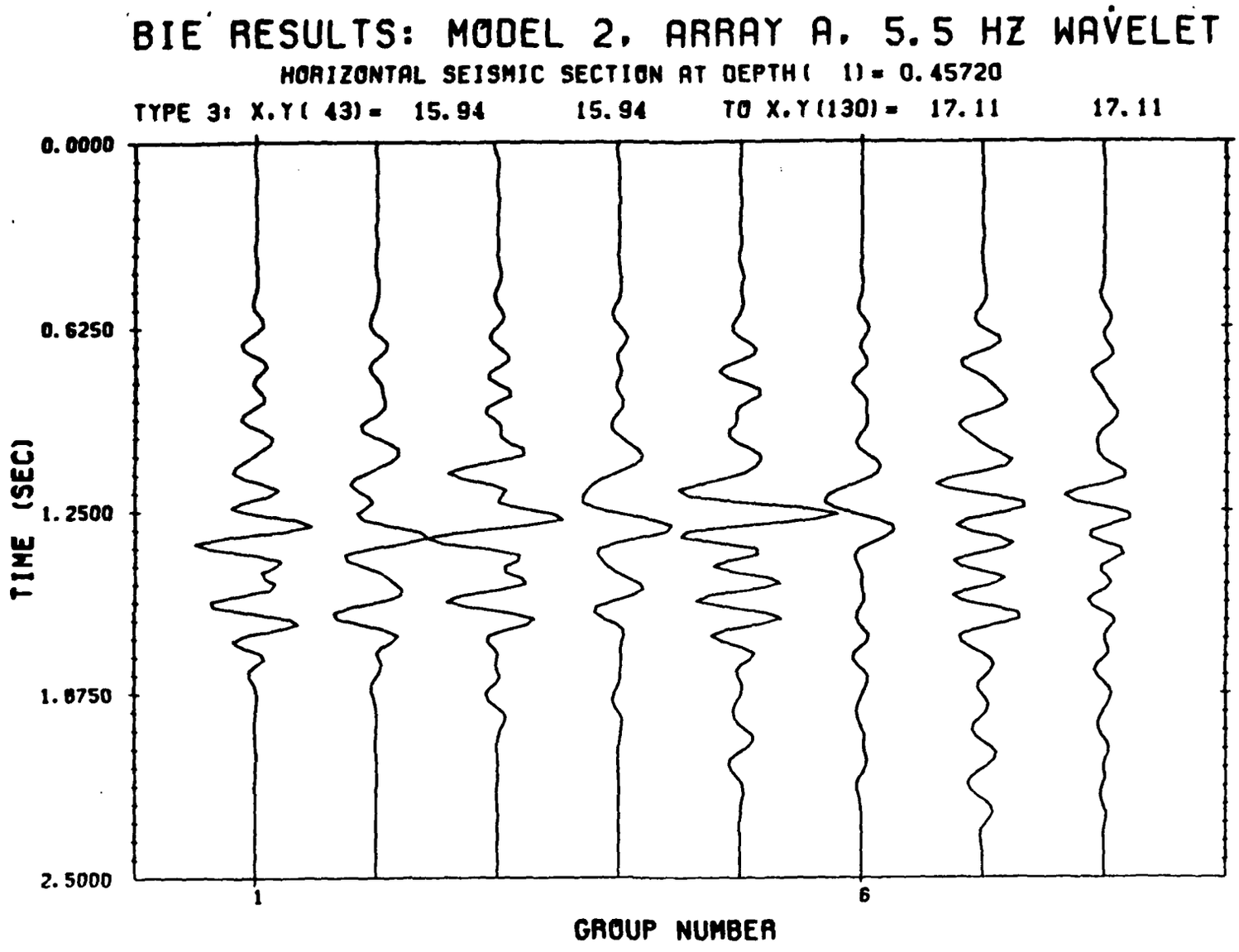

FIGURE 24. The radial and vertical components of displacement response for model 2, array A calculated by the BIE method including multiples up to third order. A 5.5 hz Ricker wavelet (Figure 10) has been convolved with the response to a pressure source of 1 N-m. The order of stations is A-1 through A-4 with alternating radial and vertical components with radial first. The time scale is reduced using a velocity of 3.2 km/s. The traces are scaled to a maximum amplitude of 1.74×10^{-15}m on trace 5 (station A-3, radial).

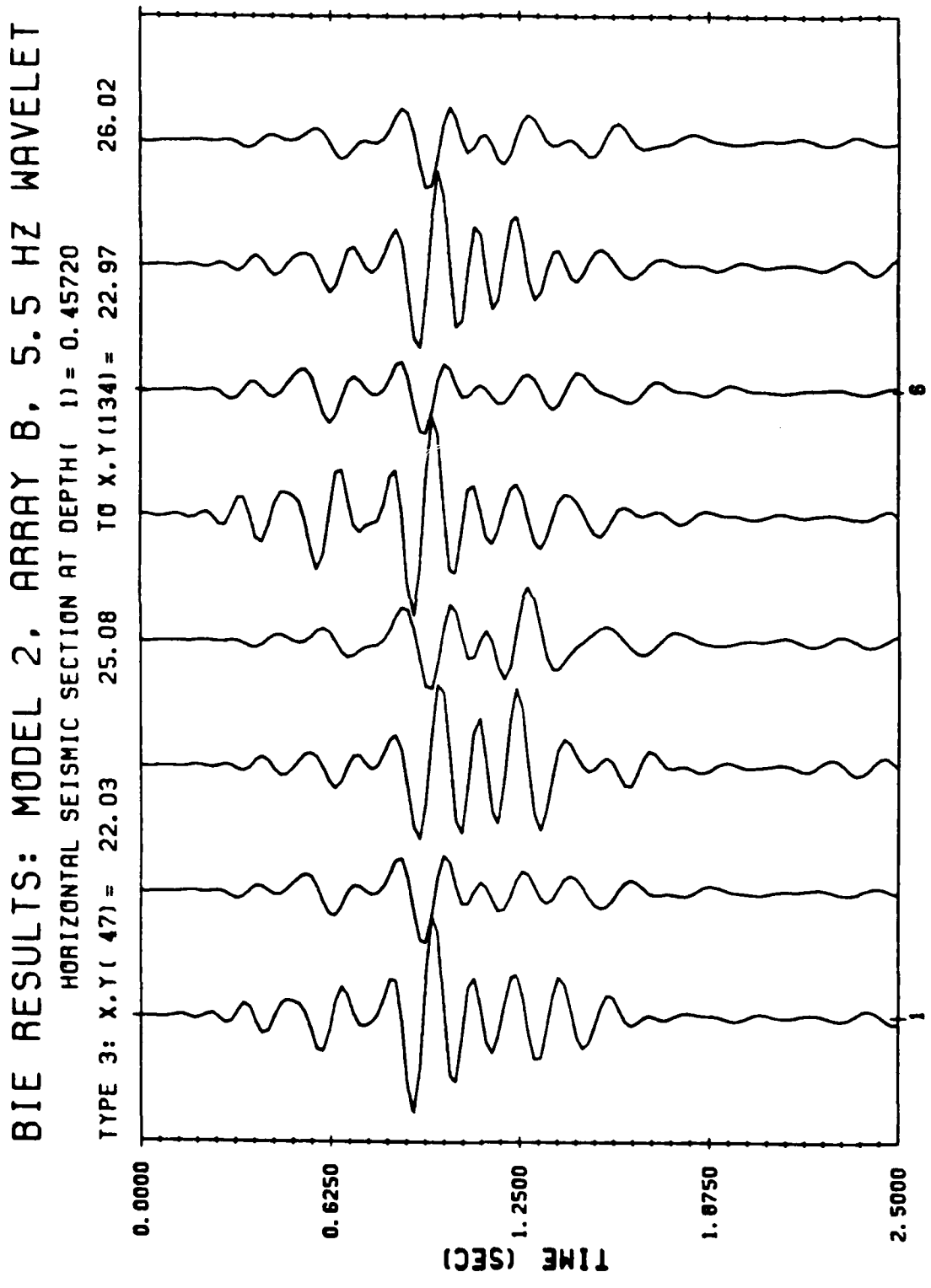

FIGURE 25. The radial and vertical displacement response for model 2, array B calculated by the BIE method including multiples to third order. See caption, Figure 24. The traces are scaled to a maximum amplitude of 2.50×10^{-15} m on trace 1 (station B-1, radial).

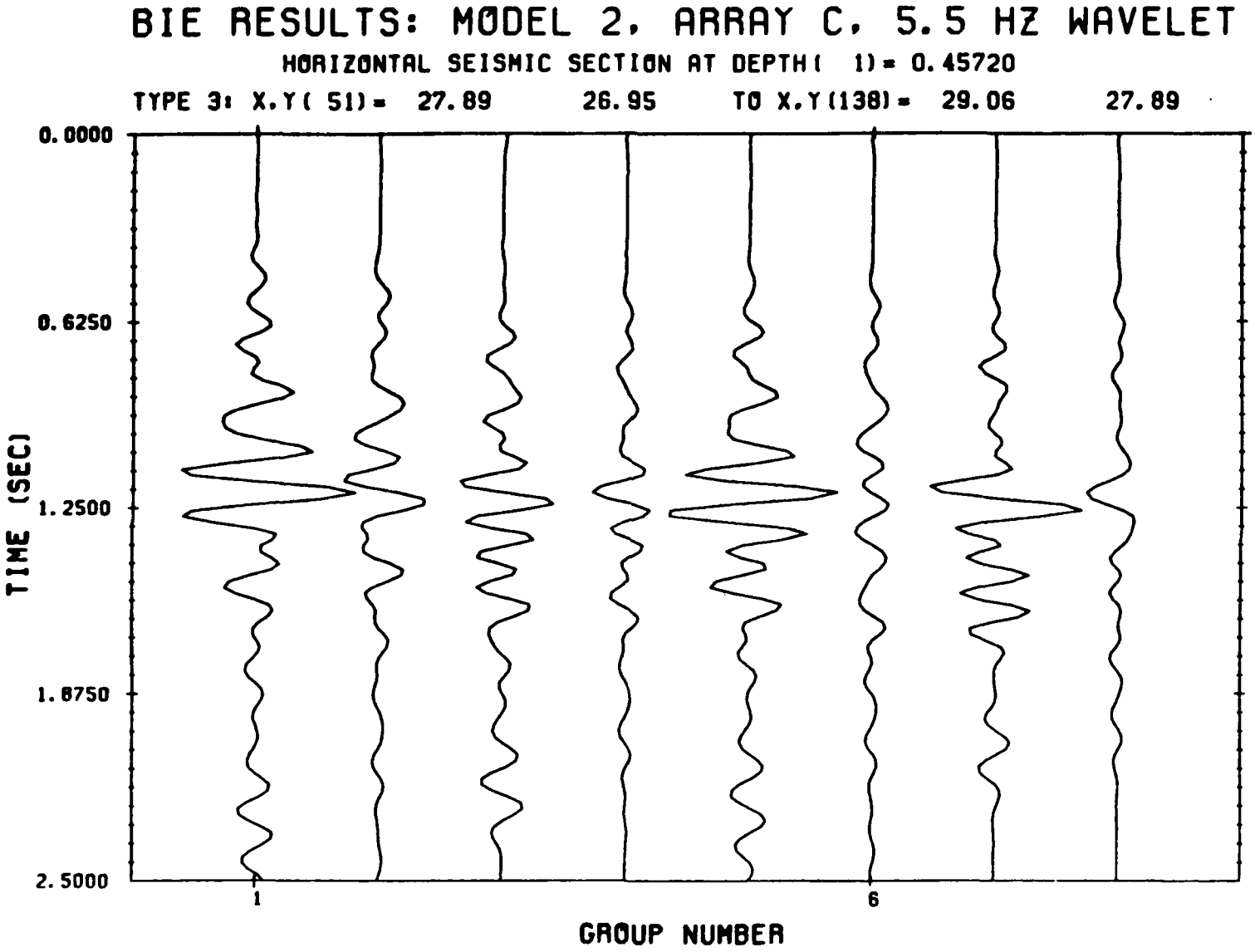

FIGURE 26 The radial and vertical components of displacement response for model 2, array C calculated by the BIE method including multiples up to third order. See caption, Figure 24. The time scale is reduced using a velocity of 3.2 km/s. The traces are scaled to 1.93 x 10^{-15} on trace 1 (station C-1 radial).

8.0 CONCLUSION AND RECOMMENDATIONS

The modeling results presented in this report represent an initial effort at calculating the response of three dimensional structures. We have successfully demonstrated that wave propagation in a limited class of acoustic models can be numerically simulated. Because the results in this report rely on acoustic models, the amplitude predictions for what are essentially surface waves must be interpreted carefully. It is expected that the Rayleigh waves will contribute to the solution as much or more than the trapped waves in the above calculations. Since these propagation modes travel at less than the S-wave velocity, the duration of large amplitude motion will be increased. The Rayleigh waves will also be most affected by the surface topography and nothing in these calculations is useful to predict these effects.

The techniques developed in this report will be useful for certain elastic problems in which multiple interaction between boundaries are not important. Problems concerning three dimensional modeling of reflection seismograms of teleseismic body waves are examples. The propagation algorithm presented in this report has proven to be economical for propagating a wavefield from one boundary to another in a three dimensional structure. It remains to develop an algorithm to efficiently compute the boundary interaction terms.

9.0 REFERENCES

Alterman, Z.S. and F.C. Karal, Jr., 1968, Propagation of elastic waves in layered media by finite difference methods, Bull. Seismol. Soc. Am., 58, 367-398

Apsel, R.J., Dynamic Green's functions for layered media and applications to boundary-value problems, Ph.D Thesis, University of California, San Diego, 349 p

Apsel, R.J., R.K. Wyss and G.R. Mellman, 1983, Three-dimensional wave propagation using boundary integral equation techniques, Sierra Geophysics Technical Report for DARPA, Contract No. N00014-81-C-0148

Apsel, R.J., G.R. Mellman and P.C. Wong, 1985, Three-dimensional wave propagation using boundary integral equation techniques, Sierra Geophysics Technical Report AFGL-TR-85-0245, ADA164498

Banaugh, R., 1962, Scattering of acoustic and elastic waves by surfaces of arbitrary shape, Ph.D Thesis, University of California, Lawrence Radiation Laboratory

Boore, D.M., 1972, Finite difference methods for seismic wave propagation in heterogeneous materials in Seismology: Surface Waves and Earth Oscillations, (Methods in Computational Physics, Vol. II), New York: Academic Press

Berryhill, J.R., 1979, Wave equation datuming, Geophysics, 44, 1329-1344

Bouchon, M., 1979, Discrete wave number representation of elastic wavefields in three-space dimensions, J. Geophys. Res., 84, 3609-3614

Cipar, J.J., 1985, (Private Communications)

Cole, D.M., 1980, A numerical boundary integral equation method for transient motions, Ph.D Thesis, California Institute of Technology, 228 p.

deHoop, A.T., 1958, Representation theorems for displacement in an elastic solid and their application to elastodynamic diffraction theory, D.Sc. Thesis, Technische Hogeschool, Delft, The Netherlands

Ferguson, J.F., Geophysical investigations of Yucca Flat, Nevada, Ph.D Thesis, Southern Methodist University

Hilterman, F.J., 1970, Three dimensional seismic modeling, Geophysics, 35, 1020-1037

Hron, F., 1971, Criteria for selection of phases in synthetic seismograms for layered media, Bull. Seismol. Soc. Am, 61, 765-799

Koslof, D.D. and E. Baysal, 1982, Forward modeling by a Fourier method, Geophysics, 47, 1402-1412

Mellman, G.R., R.S. Hart, G.M. Lundquist and D.M. Hadley, 1982, Investigations of near-source structural effects on body waves, Part I - Yucca Flats, Sierra Geophysics Technical Report for DARPA, Contract F08606-79-C-0009

Morse, P.M. and H. Feshbach, 1953, Methods of Theoretical Physics, New York, McGraw Hill Book Company, Inc., 1978 p.

Schuster, G.T., 1983, Some boundary integral equation methods and their application to seismic exploration, Ph.D Thesis, Columbia University

Scott, P.F. and D.V. Helmberger, 1983, Applications of the Kirchhoff-Helmholtz integral to problems in seismology, Geophys. J.R. astr. Soc, 72, 237-254

Stratton, J.A., 1941, Electromagnetic Theory, New York, McGraw-Hill Book Company, Inc.

Vidale, J.E., 1987, Application of two-dimensional finite-difference wave simulation to earthquakes, earth structure and seismic hazard, Ph.D Thesis, California Institute of Technology, 149 p.

END

8-87

DTIC